

# Hermite spectral method for the inelastic Boltzmann equation

Ruo Li\*, Yixiao Lu†, Yanli Wang‡

January 18, 2023

## Abstract

We propose a Hermite spectral method for the inelastic Boltzmann equation, which makes two-dimensional periodic problem computation affordable by the hardware nowadays. The new algorithm is based on a Hermite expansion, where the expansion coefficients for the VHS model are reduced into several summations and can be derived exactly. Moreover, a new collision model is built with a combination of the quadratic collision operator and a linearized collision operator, which helps us to balance the computational cost and the accuracy. Various numerical experiments, including spatially two-dimensional simulations, demonstrate the accuracy and efficiency of this numerical scheme.

**Keywords:** granular gas flow; inelastic Boltzmann equation; Hermite spectral method

## 1 Introduction

Granular materials have been paid more and more attention recently, such as sand, grains, snow, et al. Compared to the molecular particles modeled with elastic collision, the granular gases behave quite differently due to the energy dissipation during collisions. Therefore, most theories for the elastically colliding spheres fail to describe the granular gases. The Boltzmann equation, an important model in elastic theory, can also be extended to describe the behavior of granular gases. Recently, the inelastic Boltzmann equation has also been applied to model the social and biological systems [22].

Owing to the energy loss, the inelastic collision operator is fundamentally different from the elastic operator. Both analytical and numerical theories in this field are still at an early stage, and we refer the readers to a recent review [24] for some related results and open questions. Numerically, some methods have been proposed to solve the inelastic Boltzmann equation. The Direct Simulation Monte Carlo (DSMC) method [4], which is initially proposed for the elastic Boltzmann equation, has recently been extended to the inelastic case [2, 9]. It can efficiently compute the highly rarefied gas flow but does not work well in low-speed and unsteady flows. In recent years, deterministic methods have made significant progress in kinetics. For example, the Fourier spectral method [8, 21] has been applied to simulate the Boltzmann equation, and then successfully extended to the inelastic case [14, 26]. Besides, the Petrov–Galerkin spectral method has been proposed for the inelastic Boltzmann equation [15], and a unified gas-kinetic scheme is also adopted to deal with the inelastic collision of granular gases [19].

---

\*CAPT, LMAM & School of Mathematical Sciences, Peking University, Beijing, China, email: rli@math.pku.edu.cn.

†HEDPS, Center for Applied Physics and Technology & School of Mathematical Sciences, Peking University, Beijing, China, 100871, email: luyixiao@pku.edu.cn.

‡Beijing Computational Science Research Center, email: ylwang@csrc.ac.cn.

For inelastic gas flows, people are always concerned with the behavior of some macroscopic variables, especially temperature. Therefore, we focus on the Hermite spectral method, which can express the important macroscopic variables with the expansion coefficients of the first few orders. The history of the Hermite spectral method can be traced back to Grad's work [10] in 1949, which is known as the moment method. It is based on the idea to take the steady state, Maxwellian, as the weight function. Then, the distribution function is expanded using the orthogonal polynomials with the weight function, and these polynomials are just Hermite polynomials. In the past few years, great progress has been made in the application of the Hermite spectral method. An algorithm to approximate the general quadratic Boltzmann collision operator is first derived in [25]. Soon, the method is verified with the success in the simulation of rarefied gas flow [16]. Later, it has been modified and extended to the field of collisional plasma [18] and the multi-species Boltzmann equation [17].

In this paper, we develop a numerical algorithm based on the Hermite spectral method for the inelastic Boltzmann equation. Even though the Maxwellian is no longer the steady state of inelastic collisions, the Hermite spectral method maintains the advantage of easy expressions for the macroscopic variables. We first derive the algorithm of the inelastic quadratic collision term under the framework of the Hermite spectral method, where the complex calculation of the expansion coefficients for the quadratic collision term can be greatly reduced. For the VHS model, these coefficients can even be derived exactly with several summations. Next, to balance the accuracy and computational cost, a new collision model is built by combining the quadratic collision model and a linearized inelastic collision model modified from the work in [2, 7]. Following the similar lines of [16, 17], the Strang splitting method is utilized to separate the convection and collision parts. The finite volume method is applied to solve the convection term similarly to [16]. The collision term can be efficiently computed with the new collision model, which consumes much less computational cost than the original quadratic term but maintains reliable numerical accuracy.

In the numerical experiments, we first implement two important spatially homogeneous experiments in the granular gas flow, including the heating source problem [23] and Haff's cooling law [11]. Then the tests of one-dimensional benchmark problems are carried out, including the Couette flow and Fourier heat transfer. Finally, a two-dimensional periodic diffusion is simulated to further validate the accuracy and efficiency of the method. An excellent agreement can be observed between the numerical solution and the reference solution of the direct simulation Monte Carlo (DSMC) method.

The rest of this paper is organized as follows: in Sec. 2, we introduce the inelastic collision operator and the general framework of the Hermite spectral method. The algorithm to discretize the collision term and the special simplification for the VHS model are given in Sec. 3. The whole numerical scheme is completed in Sec. 4 with numerical experiments presented in Sec. 5. The paper ends with some concluding remarks in Sec. 6 and several supplementary contents in the Appendix.

## 2 Inelastic Boltzmann equation and Hermite spectral method

In this section, we will first give a brief review of the Boltzmann equation and the inelastic collision model, and then introduce the general framework for solving the Boltzmann equation using Hermite spectral method.

## 2.1 Inelastic Boltzmann equation

The inelastic Boltzmann equation is always utilized to describe the granular gas flow, whose nondimensionalized form [5] is

$$\frac{\partial f}{\partial t} + \mathbf{v} \cdot \nabla_{\mathbf{x}} f = \frac{1}{\text{Kn}} \mathcal{Q}[f, f](\mathbf{v}), \quad (2.1)$$

where  $f(t, \mathbf{x}, \mathbf{v})$  is the distribution function, which depends on time  $t \in \mathbb{R}^+$ , physical space  $\mathbf{x} \in \mathbb{R}^3$  and particle velocity  $\mathbf{v} \in \mathbb{R}^3$ . Kn is the Knudsen number indicating the ratio of the mean free path to  $\mathcal{Q}$  is the quadratic inelastic collision operator, which takes the form

$$\mathcal{Q}[f, f](\mathbf{v}) = \int_{\mathbb{R}^3} \int_{S^2} [B(|\tilde{\mathbf{g}}|, \sigma) f(\tilde{\mathbf{v}}) f(\tilde{\mathbf{v}}_*) J - B(|\mathbf{g}|, \sigma) f(\mathbf{v}) f(\mathbf{v}_*)] d\sigma d\mathbf{v}_*. \quad (2.2)$$

This collision operator describes the inelastic collision between two particles. Suppose two particles with velocity pair  $(\mathbf{v}, \mathbf{v}_*)$  are going to collide. Under the assumption of inelastic collision, the post-collision velocity pair  $(\mathbf{v}', \mathbf{v}'_*)$  can be expressed as [5]

$$\begin{cases} \mathbf{v}' = \frac{\mathbf{v} + \mathbf{v}_*}{2} + \frac{1-e}{4}(\mathbf{v} - \mathbf{v}_*) + \frac{1+e}{4}|\mathbf{v} - \mathbf{v}_*|\sigma, \\ \mathbf{v}'_* = \frac{\mathbf{v} + \mathbf{v}_*}{2} - \frac{1-e}{4}(\mathbf{v} - \mathbf{v}_*) - \frac{1+e}{4}|\mathbf{v} - \mathbf{v}_*|\sigma, \end{cases} \quad (2.3)$$

where  $\sigma$  is a unit vector in  $S^2$ ,  $e \in [0, 1]$  is the restitution coefficient indicating the inelasticity. During the collisions, we can derive the conservation of momentum

$$\mathbf{v} + \mathbf{v}_* = \mathbf{v}' + \mathbf{v}'_*, \quad (2.4)$$

and the dissipation of energy

$$|\mathbf{v}|^2 + |\mathbf{v}_*|^2 - (|\mathbf{v}'|^2 + |\mathbf{v}'_*|^2) = \frac{1-e^2}{4} |\mathbf{g}|(|\mathbf{g}| - \mathbf{g} \cdot \sigma), \quad (2.5)$$

where  $\mathbf{g} = \mathbf{v} - \mathbf{v}_*$  is the relative velocity. Define the pre-collisional velocities  $(\tilde{\mathbf{v}}, \tilde{\mathbf{v}}_*)$  as the velocity pair which will turn into  $(\mathbf{v}, \mathbf{v}_*)$  following the rule in (2.3) with the collision of parameter  $\sigma$ . Here, we want to emphasize that, unlike the elastic case,  $(\tilde{\mathbf{v}}, \tilde{\mathbf{v}}_*)$  does not coincide with  $(\mathbf{v}', \mathbf{v}'_*)$ , and the collisions are not reversible. We define  $\tilde{\mathbf{g}} = \tilde{\mathbf{v}} - \tilde{\mathbf{v}}_*$  as the relative velocity of the pre-collisional velocities, and  $J = \left| \frac{\partial(\tilde{\mathbf{v}}, \tilde{\mathbf{v}}_*)}{\partial(\mathbf{v}, \mathbf{v}_*)} \right|$  the determinant of the Jacobian. In (2.2),  $B$  is the collision kernel which depends on the type of interactions. The most commonly used form for the inelastic case is the variable hard sphere (VHS) model [4]:

$$B(|\mathbf{g}|, \sigma) = C_{\varpi} |\mathbf{g}|^{2(1-\varpi)}, \quad (2.6)$$

where  $C_{\varpi} > 0$  and  $0.5 \leq \varpi \leq 1$  are some constants. Especially, the Maxwell molecules and hard sphere model (HS) are corresponding to  $\varpi = 0.5$  and  $\varpi = 1$  respectively.

To derive the weak form of (4.16), multiplying a test function  $\phi(\mathbf{v})$  and taking integral on  $\mathbf{v}$ , it holds that [14]

$$\int_{\mathbb{R}^3} \mathcal{Q}[f, f](\mathbf{v}) \phi(\mathbf{v}) d\mathbf{v} = \int_{\mathbb{R}^3} \int_{\mathbb{R}^3} \int_{S^2} B(|\mathbf{g}|, \sigma) f(\mathbf{v}) f(\mathbf{v}_*) [\phi(\mathbf{v}') - \phi(\mathbf{v})] d\sigma d\mathbf{v} d\mathbf{v}_*, \quad (2.7)$$

which has a more symmetric form as

$$\begin{aligned} & \int_{\mathbb{R}^3} \mathcal{Q}[f, f](\mathbf{v}) \phi(\mathbf{v}) d\mathbf{v} \\ &= \frac{1}{2} \int_{\mathbb{R}^3} \int_{\mathbb{R}^3} \int_{S^2} B(|\mathbf{g}|, \sigma) f(\mathbf{v}) f(\mathbf{v}_*) [\phi(\mathbf{v}') + \phi(\mathbf{v}'_*) - \phi(\mathbf{v}) - \phi(\mathbf{v}_*)] d\sigma d\mathbf{v} d\mathbf{v}_*. \end{aligned} \quad (2.8)$$

We refer [14] for the derivation of this weak form. Specifically,  $\phi(\mathbf{v})$  can be chosen as any polynomial of  $\mathbf{v}$ , which is quite important in the framework of the Hermite spectral method to discretize the collision operator. Especially, let  $\phi = |\mathbf{v}|^2$ , From (2.8) and (2.5), we can derive that the inelastic collision does not conserve the total energy as

$$\int_{\mathbb{R}^3} \mathcal{Q}[f, f](\mathbf{v}) |\mathbf{v}|^2 d\mathbf{v} < 0. \quad (2.9)$$

Due to the complex form of the quadratic collision operator, several simplified collision models are proposed. Since the total energy is not conserved during the inelastic collision, the BGK collision model [3] does not work well in the inelastic case. In [7, (3.12)], a linearized collision term with energy dissipation is constructed with

$$\mathcal{Q}_{\text{lin}}(\mathbf{v}) = \nu_1 \tau(P) [f_G(\mathbf{v}) - f(\mathbf{v})] + \nu_2 \nabla_{\mathbf{v}} \cdot [(\mathbf{v} - \mathbf{u}) f(\mathbf{v})], \quad (2.10)$$

where the parameters  $\nu_1$  and  $\nu_2$  is problem dependent. In [7],  $\nu_1 = \tau(P)$ , where  $\tau(\cdot)$  is a given function depending on the kinetic pressure  $P := \rho\theta$  and  $\nu_2 = C\rho\theta^{1/2}$  with  $C$  a given constant. A similar model is also proposed in [2, (2.20)], which contains the same energy loss term, but with different parameters  $\nu_2$ . The first term in (2.10) is the ellipsoidal statistical BGK (ES-BGK) operator, which has the form [13]

$$\begin{aligned} f_G &= \frac{\rho}{|2\pi\Lambda|} \exp\left(-\frac{1}{2}(\mathbf{v} - \mathbf{u})^T \Lambda (\mathbf{v} - \mathbf{u})\right), \\ \Lambda &= (\lambda_{ij}) \in \mathbb{R}^{3 \times 3}, \quad \lambda_{ij} = \frac{1}{\text{Pr}} \theta \delta_{ij} + \left(1 - \frac{1}{\text{Pr}}\right) \frac{\sigma_{ij} + \delta_{ij} \rho \theta}{\rho}, \end{aligned} \quad (2.11)$$

where  $\delta_{ij}$  is the Kronecker delta,  $\text{Pr}$  is the Prandtl number, which takes the value  $\frac{2}{3}$  for monatomic gas.  $\rho, \mathbf{u}, \theta$  and  $\boldsymbol{\sigma}$  are the density, macroscopic velocity, temperature and stress tensor, respectively, whose relationships with the distribution function are

$$\begin{aligned} \rho(t, \mathbf{x}) &= \int_{\mathbb{R}^3} f(t, \mathbf{x}, \mathbf{v}) d\mathbf{v}, \quad \mathbf{u}(t, \mathbf{x}) = \frac{1}{\rho} \int_{\mathbb{R}^3} \mathbf{v} f(t, \mathbf{x}, \mathbf{v}) d\mathbf{v}, \\ 3\theta(t, \mathbf{x})\rho(t, \mathbf{x}) &= \int_{\mathbb{R}^3} |\mathbf{v} - \mathbf{u}|^2 f(t, \mathbf{x}, \mathbf{v}) d\mathbf{v}, \\ \boldsymbol{\sigma}(t, \mathbf{x}) &= \int_{\mathbb{R}^3} \left[ (\mathbf{v} - \mathbf{u}) \otimes (\mathbf{v} - \mathbf{u}) - \frac{1}{3} |\mathbf{v} - \mathbf{u}|^2 I \right] f(t, \mathbf{x}, \mathbf{v}) d\mathbf{v}. \end{aligned} \quad (2.12)$$

Moreover, the heat flux  $\mathbf{q}$  could be derived from the distribution function as

$$\mathbf{q}(t, \mathbf{x}) = \frac{1}{2} \int_{\mathbb{R}^3} (\mathbf{v} - \mathbf{u}) |\mathbf{v} - \mathbf{u}|^2 f(t, \mathbf{x}, \mathbf{v}) d\mathbf{v}. \quad (2.13)$$

For now, we have introduced the inelastic Boltzmann equation. Due to its high dimensionality and the complex collision term, it is always a challenge to solve it numerically. Several numerical methods have been proposed to deal with the inelastic Boltzmann equation, such as the DSMC method [2, 9], the Fourier spectral method [14, 26] and the Petrov–Galerkin spectral method [15]. In this work, we will develop a numerical scheme based on the Hermite spectral method, which may handle the evolution of temperature more accurately than other methods.

## 2.2 Hermite spectral method

This subsection presents the general framework for solving the inelastic Boltzmann equation using the Hermite spectral method. We begin from the local Maxwellian as

$$\mathcal{M}_{\mathbf{u},\theta}(\mathbf{v}) = \frac{\rho}{(2\pi\theta)^{\frac{3}{2}}} \exp\left(-\frac{|\mathbf{v} - \mathbf{u}|^2}{2\theta}\right), \quad (2.14)$$

which is the steady-state solution to the elastic case ( $e = 1$  in (2.3)). Here,  $\rho, \mathbf{u}, \theta$  are the density, macroscopic velocity and temperature defined in (2.12), respectively. The Hermite spectral method is successfully utilized to solve the elastic Boltzmann equation [16, 25], where the local Maxwellian (2.14) is adopted as the weight function to generate orthogonal polynomials (i.e. Hermite polynomials), which are utilized as the basis polynomials. Precisely, assuming the expansion center is  $[\bar{\mathbf{u}}, \bar{\theta}] \in \mathbb{R}^3 \times \mathbb{R}^+$ , then the weight function has the form as

$$\omega_{\bar{\mathbf{u}},\bar{\theta}}(\mathbf{v}) = \frac{1}{(2\pi\bar{\theta})^{\frac{3}{2}}} \exp\left(-\frac{|\mathbf{v} - \bar{\mathbf{u}}|^2}{2\bar{\theta}}\right), \quad (2.15)$$

and the corresponding Hermite polynomials are defined as

**Definition** (Hermite Polynomials). For  $\alpha = (\alpha_1, \alpha_2, \alpha_3) \in \mathbb{N}^3$ , the three-dimensional Hermite polynomial  $H_{\alpha}^{\bar{\mathbf{u}},\bar{\theta}}(\mathbf{v})$  is defined as

$$H_{\alpha}^{\bar{\mathbf{u}},\bar{\theta}}(\mathbf{v}) = \frac{(-1)^{|\alpha|} \bar{\theta}^{\frac{|\alpha|}{2}}}{\omega_{\bar{\mathbf{u}},\bar{\theta}}(\mathbf{v})} \frac{\partial^{|\alpha|}}{\partial \mathbf{v}^{\alpha}} \omega_{\bar{\mathbf{u}},\bar{\theta}}(\mathbf{v}), \quad (2.16)$$

with  $|\alpha| = \alpha_1 + \alpha_2 + \alpha_3$  and  $\partial \mathbf{v}^{\alpha} = \partial v_1^{\alpha_1} \partial v_2^{\alpha_2} \partial v_3^{\alpha_3}$ . The Hermite polynomials have several useful properties when approximating the complex collision term, which is listed in Appendix F.

Then following the similar routine in [25], the distribution function  $f(t, \mathbf{x}, \mathbf{v})$  is approximated as

$$f(t, \mathbf{x}, \mathbf{v}) \approx \sum_{|\alpha| \leq M} f_{\alpha}^{[\bar{\mathbf{u}},\bar{\theta}]}(t, \mathbf{x}) \mathcal{H}_{\alpha}^{\bar{\mathbf{u}},\bar{\theta}}(\mathbf{v}), \quad (2.17)$$

where  $\mathcal{H}_{\alpha}^{\bar{\mathbf{u}},\bar{\theta}}(\mathbf{v}) = H_{\alpha}^{\bar{\mathbf{u}},\bar{\theta}}(\mathbf{v}) \omega_{\bar{\mathbf{u}},\bar{\theta}}(\mathbf{v})$  are the basis functions.  $|\alpha| = \alpha_1 + \alpha_2 + \alpha_3$  and  $M \in \mathbb{N}$  is the expansion order. Here, we want to emphasize that with a properly chosen expansion center, the computational cost may be greatly reduced. In practice, the expansion center is often chosen as a rough average of the whole domain to ensure numerical accuracy. With the orthogonality of the basis function (F.1), it holds

$$f_{\alpha}^{[\bar{\mathbf{u}},\bar{\theta}]}(t, \mathbf{x}) = \frac{1}{\alpha!} \int_{\mathbb{R}^3} f(t, \mathbf{x}, \mathbf{v}) H_{\alpha}^{\bar{\mathbf{u}},\bar{\theta}}(\mathbf{v}) d\mathbf{v}. \quad (2.18)$$

With the expansion (2.17), the macroscopic variables in (2.12), (2.13) could be expressed with  $f_{\alpha}^{[\bar{\mathbf{u}},\bar{\theta}]}$  as

$$\begin{aligned} \rho &= f_0^{[\bar{\mathbf{u}},\bar{\theta}]}, \quad u_k = \bar{u}_k + \frac{\sqrt{\bar{\theta}}}{\rho} f_{e_k}^{[\bar{\mathbf{u}},\bar{\theta}]}, \quad \theta = \frac{2\bar{\theta}}{3\rho} \sum_{k=1}^3 f_{2e_k}^{[\bar{\mathbf{u}},\bar{\theta}]} + \bar{\theta} - \frac{1}{3\rho} |\mathbf{u} - \bar{\mathbf{u}}|^2, \\ \sigma_{kl} &= (1 + \delta_{kl}) \bar{\theta} f_{e_i+e_j}^{[\bar{\mathbf{u}},\bar{\theta}]} + \delta_{kl} \rho (\bar{\theta} - \theta) - \rho (\bar{u}_k - u_k) (\bar{u}_l - u_l), \\ q_k &= 2\bar{\theta}^{\frac{3}{2}} f_{3e_k}^{[\bar{\mathbf{u}},\bar{\theta}]} + (\bar{u}_k - u_k) \bar{\theta} f_{2e_k}^{[\bar{\mathbf{u}},\bar{\theta}]} + |\bar{\mathbf{u}} - \mathbf{u}|^2 \sqrt{\bar{\theta}} f_{e_k}^{[\bar{\mathbf{u}},\bar{\theta}]} + \\ &\quad \sum_{l=1}^3 \left[ \bar{\theta}^{\frac{3}{2}} f_{2e_l+e_k}^{[\bar{\mathbf{u}},\bar{\theta}]} + (\bar{u}_l - u_l) \bar{\theta} f_{e_l+e_k}^{[\bar{\mathbf{u}},\bar{\theta}]} + (\bar{u}_k - u_k) \bar{\theta} f_{2e_l}^{[\bar{\mathbf{u}},\bar{\theta}]} \right], \quad k, l = 1, 2, 3. \end{aligned} \quad (2.19)$$

Moreover, if the expansion center is chosen as the local macroscopic velocity and temperature as  $[\bar{\mathbf{u}}, \bar{\theta}] = [\mathbf{u}, \theta]$ , then (2.19) is reduced into

$$f_{e_k}^{[\mathbf{u}, \theta]} = 0, \quad \sum_{k=1}^3 f_{2e_k}^{[\mathbf{u}, \theta]} = 0, \quad \sigma_{kl} = (1 + \delta_{kl})\theta f_{e_i+e_j}^{[\mathbf{u}, \theta]}, \quad q_k = \theta^{\frac{3}{2}} \left[ 2f_{3e_k}^{[\mathbf{u}, \theta]} + \sum_{l=1}^3 f_{2e_l+e_k}^{[\mathbf{u}, \theta]} \right]. \quad (2.20)$$

Therefore, the macroscopic quantities could be easily obtained under the framework of the Hermite spectral method. This is to say, we are able to govern the evolution of some important macroscopic variables with a small  $M$ .

For the collision term, it is also expanded using the same basis functions and approximated as

$$\mathcal{Q}[f, f](\mathbf{v}) \approx \sum_{|\alpha| \leq M} Q_\alpha^{[\bar{\mathbf{u}}, \bar{\theta}]}(t, \mathbf{x}) \mathcal{H}_\alpha^{\bar{\mathbf{u}}, \bar{\theta}}(\mathbf{v}), \quad Q_\alpha^{[\bar{\mathbf{u}}, \bar{\theta}]}(t, \mathbf{x}) = \frac{1}{\alpha!} \int_{\mathbb{R}^3} \mathcal{Q}[f, f](\mathbf{v}) H_\alpha^{\bar{\mathbf{u}}, \bar{\theta}}(\mathbf{v}) d\mathbf{v}. \quad (2.21)$$

Then, substituting the expansion (2.17), (2.21) into (2.1) and matching the coefficients on both sides, the moment equations could be derived as

$$\frac{\partial}{\partial t} f_\alpha^{[\bar{\mathbf{u}}, \bar{\theta}]} + \sum_{d=1}^3 \frac{\partial}{\partial x_d} \left( (\alpha_d + 1) \sqrt{\bar{\theta}} f_{\alpha+e_d}^{[\bar{\mathbf{u}}, \bar{\theta}]} + \bar{u}_d f_\alpha^{[\bar{\mathbf{u}}, \bar{\theta}]} + \sqrt{\bar{\theta}} f_{\alpha-e_d}^{[\bar{\mathbf{u}}, \bar{\theta}]} \right) = Q_\alpha^{[\bar{\mathbf{u}}, \bar{\theta}]}, \quad |\alpha| \leq M, \quad (2.22)$$

where the recurrence relationship (F.3) is utilized to deal with the convection term. In (2.22),  $f_\alpha^{[\bar{\mathbf{u}}, \bar{\theta}]}$  is regarded as 0 if  $\alpha$  contains any negative index or  $|\alpha| > M$ .

For now, we have derived the moment equations for the Boltzmann equation. The main difficulty to solve (2.22) lies in the approximation of  $Q_\alpha^{[\bar{\mathbf{u}}, \bar{\theta}]}(t, \mathbf{x})$  in (2.21), which will be discussed in detail in the following section.

### 3 Approximation of the collision terms

In this section, we introduce the approximation of the collision term in the framework of the Hermite spectral method. The discretization of the quadratic term is discussed in Sec. 3.1, and the simplification of the VHS model is presented in Sec. 3.2.

#### 3.1 Series expansion of general collision terms

We first discuss the algorithm to calculate the expansion coefficients  $Q_\alpha^{[\bar{\mathbf{u}}, \bar{\theta}]}(t, \mathbf{x})$  of the quadratic collision term in (2.21). Without loss of generality, we suppose the expansion center  $[\bar{\mathbf{u}}, \bar{\theta}] = [\mathbf{0}, 1]$  and omit the superscript  $\bar{\mathbf{u}}, \bar{\theta}$  for simplicity as

$$f_\alpha(t, \mathbf{x}) = f_\alpha^{[0,1]}(t, \mathbf{x}), \quad Q_\alpha(t, \mathbf{x}) = Q_\alpha^{[0,1]}(t, \mathbf{x}), \quad H_\alpha(\mathbf{v}) = H_\alpha^{0,1}(\mathbf{v}), \quad \omega(\mathbf{v}) = \omega_{0,1}(\mathbf{v}). \quad (3.1)$$

With the weak form (2.7), we can simplify (2.21) as

$$Q_\alpha(t, \mathbf{x}) = \int_{\mathbb{R}^3} \int_{\mathbb{R}^3} \int_{S^2} B(|\mathbf{g}|, \sigma) f(\mathbf{v}) f(\mathbf{v}_*) [H_\alpha(\mathbf{v}') - H_\alpha(\mathbf{v})] d\sigma d\mathbf{v} d\mathbf{v}_*. \quad (3.2)$$

Substituting the expansion of the distribution function (2.17) into (3.2), we can deduce that

$$Q_\alpha(t, \mathbf{x}) = \sum_{|\lambda| \leq M} \sum_{|\kappa| \leq M} A_{\alpha, \lambda, \kappa} f_\lambda f_\kappa, \quad (3.3)$$

with

$$A_{\alpha,\lambda,\kappa} = \frac{1}{\alpha!} \int_{\mathbb{R}^3} \int_{\mathbb{R}^3} \int_{S^2} B(|\mathbf{g}|, \sigma) \mathcal{H}_\lambda(\mathbf{v}) \mathcal{H}_\kappa(\mathbf{v}_*) [H_\alpha(\mathbf{v}') - H_\alpha(\mathbf{v})] d\sigma d\mathbf{v} d\mathbf{v}_*. \quad (3.4)$$

With the properties of Hermite polynomials, the calculation of  $A_{\alpha,\lambda,\kappa}$  can be greatly simplified and the result is listed in Theorem 1.

**Theorem 1.** *The coefficients  $A_{\alpha,\lambda,\kappa}$  have the form below:*

$$A_{\alpha,\lambda,\kappa} = \frac{1}{2^{\frac{|\alpha|+3}{2}}} \sum_{\lambda' \preceq \alpha, \lambda' \preceq \kappa + \lambda} \frac{1}{\mathbf{j}!} a_{l'_1 k'_1}^{l_1 k_1} a_{l'_2 k'_2}^{l_2 k_2} a_{l'_3 k'_3}^{l_3 k_3} \gamma_{\kappa'}^{\mathbf{j}}, \quad (3.5)$$

where  $\kappa' = \kappa + \lambda - \lambda'$ ,  $\mathbf{j} = \alpha - \lambda'$ , and the symbol ' $\preceq$ ' means

$$(i_1, i_2, i_3) \preceq (j_1, j_2, j_3) \Leftrightarrow i_s \leq j_s \quad \text{for } s = 1, 2, 3.$$

Besides, the coefficients  $a_{l'_d k'_d}^{l_d k_d}$  and  $\gamma_{\kappa}^{\mathbf{j}}$  in (3.5) are given by

$$a_{l'_d k'_d}^{l_d k_d} = 2^{-\frac{l'_d + k'_d}{2}} \sum_{s \in \mathbb{Z}} C_{l_d}^s C_{k_d}^{l'_d - s} (-1)^{k_d - l'_d + s}, \quad (3.6)$$

and

$$\gamma_{\kappa}^{\mathbf{j}} = \int_{\mathbb{R}^3} \int_{S^2} \left[ H_{\mathbf{j}} \left( \frac{\mathbf{g}'}{\sqrt{2}} \right) - H_{\mathbf{j}} \left( \frac{\mathbf{g}}{\sqrt{2}} \right) \right] H_{\kappa} \left( \frac{\mathbf{g}}{\sqrt{2}} \right) B(|\mathbf{g}|, \sigma) \omega \left( \frac{\mathbf{g}}{\sqrt{2}} \right) d\sigma d\mathbf{g}, \quad (3.7)$$

where from (2.3), it hold that for  $\mathbf{g}'$  that

$$\mathbf{g}' \triangleq \mathbf{v}' - \mathbf{v}_* = \frac{1-e}{2} \mathbf{g} + \frac{1+e}{2} |\mathbf{g}| \sigma. \quad (3.8)$$

The proof of Theorem 1 is similar to [25, Theorem 1]. For the completeness of this work, we put it in App. A. Different from the classical case,  $|\mathbf{g}'|$  does not equal  $|\mathbf{g}|$  in the inelastic model, therefore,  $\gamma_{\kappa}^{\mathbf{j}}$  could not be further simplified as in [25]. But for the special collision kernel such as the VHS kernel, (3.7) could be calculated exactly, which will be discussed in the next section.

### 3.2 Simplification of VHS model

For the VHS kernel (2.6), which does not depend on the collision parameter  $\sigma$ , the coefficient (3.7) could be calculated exactly. We will begin from two lemmas below as

**Lemma 1.** *Assuming  $\sigma = (\sigma_1, \sigma_2, \sigma_3)$  is a unit vector.  $\kappa = (\kappa_1, \kappa_2, \kappa_3) \in \mathbb{N}^3$ . Then the integral in the unit sphere holds*

$$\mathcal{S}(\kappa) \triangleq \int_{S^2} \sigma_1^{\kappa_1} \sigma_2^{\kappa_2} \sigma_3^{\kappa_3} d\sigma = \begin{cases} 4\pi \frac{(\kappa-1)!!}{(|\kappa|+1)!!}, & 2|\kappa|, \\ 0, & \text{otherwise,} \end{cases} \quad (3.9)$$

where  $(-1)!!$  is regarded as 1,  $\kappa!! = \kappa_1!! \kappa_2!! \kappa_3!!$ , and  $2|\kappa|$  means all the components of  $\kappa$  are even.

*Proof of Lemma 1.* The proof can be completed with a spherical coordinate transform.  $\square$

**Lemma 2.** For the Hermite polynomial  $H_\alpha(\mathbf{v})$  and the weight function  $\omega(\mathbf{v})$  defined in (3.1), it holds that

$$\begin{aligned}\mathcal{V}(\kappa, \alpha, \mu) &\triangleq \int_{\mathbb{R}^3} \mathbf{v}^\kappa H_\alpha(\mathbf{v}) |\mathbf{v}|^\mu \omega(\mathbf{v}) d\mathbf{v} \\ &= (2\pi)^{-\frac{3}{2}} \sum_{\substack{\mathbf{j} \preceq \alpha \\ 2|(\alpha - \mathbf{j})}} \mathcal{C}(\alpha, \mathbf{j}) 2^{\frac{1+\mu+|\mathbf{j}|+|\kappa|}{2}} \Gamma\left(\frac{3+\mu+|\mathbf{j}|+|\kappa|}{2}\right) \mathcal{S}(\mathbf{j} + \kappa),\end{aligned}\quad (3.10)$$

where  $\alpha, \kappa \in \mathbb{N}^3$  and  $\mu \in \mathbb{R}^+$ .  $\Gamma(\cdot)$  is the Gamma function and

$$\mathcal{C}(\alpha, \beta) = \mathcal{C}(\alpha_1, \beta_1) \mathcal{C}(\alpha_2, \beta_2) \mathcal{C}(\alpha_3, \beta_3) \quad (3.11)$$

with  $\mathcal{C}(n, k)$ ,  $n, k \in \mathbb{N}$  the coefficient of  $x^k$  in  $H_n(x)$ .

The proof of Lemma 2 is listed in App. B. Defining the coefficients  $D(\alpha, \beta, \mu)$  and  $\psi(\alpha, \beta, \mu)$  as

$$D(\alpha, \beta, \mu) = \int_{\mathbb{R}^3} \int_{S^2} H_\alpha(\mathbf{g}') H_\beta(\mathbf{g}) |\mathbf{g}|^\mu \omega(\mathbf{g}) d\sigma d\mathbf{g}, \quad (3.12)$$

$$\psi(\alpha, \beta, \mu) = \int_{\mathbb{R}^3} \int_{S^2} H_\alpha(\mathbf{g}) H_\beta(\mathbf{g}) |\mathbf{g}|^\mu \omega(\mathbf{g}) d\sigma d\mathbf{g}, \quad (3.13)$$

then the following theorem holds for the VHS model as

**Theorem 2.** For the VHS kernel  $B(|\mathbf{g}|, \sigma) = C|\mathbf{g}|^{2(1-\varpi)}$ , (3.7) could be calculated exactly as

$$\gamma_\kappa^{\mathbf{j}} = C 2^{\frac{5}{2}-\varpi} \left[ D(\mathbf{j}, \kappa, 2(1-\varpi)) - \psi(\mathbf{j}, \kappa, 2(1-\varpi)) \right]. \quad (3.14)$$

*Proof of Theorem 2.* Applying the change of variables  $\mathbf{g} \rightarrow \sqrt{2}\mathbf{g}$ , (3.7) can be simplified into (3.14) with (3.12) and (3.13).  $\square$

For now, the point left is how to calculate  $D(\alpha, \beta, \mu)$  and  $\psi(\alpha, \beta, \mu)$  in (3.12) and (3.13), which is proposed in the Proposition below, and the proof is listed in App. B.

**Proposition 3.** The coefficients  $D(\alpha, \beta, \mu)$ , and  $\psi(\alpha, \beta, \mu)$  in (3.12) and (3.13) can be calculated exactly as

$$D(\alpha, \beta, \mu) = \sum_{\substack{\lambda \preceq \alpha \\ 2|(\alpha - \lambda)}} \mathcal{C}(\alpha, \lambda) \sum_{\substack{\kappa \preceq \lambda \\ 2|(\lambda - \kappa)}} C_\lambda^\kappa \left(\frac{1-e}{2}\right)^{|\kappa|} \left(\frac{1+e}{2}\right)^{|\lambda|-|\kappa|} \mathcal{S}(\lambda - \kappa) \mathcal{V}(\kappa, \beta, |\lambda| - |\kappa| + \mu), \quad (3.15)$$

where

$$C_\lambda^\kappa = C_{\lambda_1}^{\kappa_1} C_{\lambda_2}^{\kappa_2} C_{\lambda_3}^{\kappa_3}, \quad C_m^n = \frac{m!}{n!(m-n)!}, \quad (3.16)$$

and

$$\psi(\alpha, \beta, \mu) = 4\pi \sum_{\substack{\lambda \preceq \alpha \\ 2|(\alpha - \lambda)}} \mathcal{C}(\alpha, \lambda) \mathcal{V}(\lambda, \beta, \mu). \quad (3.17)$$

For Maxwell molecules ( $\varpi = 1$ ), since the collision kernel  $B$  does not depend on  $\mathbf{g}$ , there are special sparsity for the coefficient  $A_{\alpha, \lambda, \kappa}$ . Thus, we have the following proposition of  $A_{\alpha, \lambda, \kappa}$ , and the proof is listed in App. B.



Coefficients	Formula	Used in	Computational cost
$\mathcal{S}(\kappa)$	(3.9)	(3.10), (3.15)	$\mathcal{O}(M^3)$
$\mathcal{V}(\kappa, \alpha, \mu)$	(3.10)	(3.15), (3.17)	$\mathcal{O}(M^{10})$
$D(\alpha, \beta, \mu)$	(3.12)	(3.14)	$\mathcal{O}(M^9)$
$\psi(\alpha, \beta, \mu)$	(3.13)	(3.14)	$\mathcal{O}(M^9)$
$\gamma_\kappa^j$	(3.7)	(3.5)	$\mathcal{O}(M^6)$
$a_{l'_d k'_d}^{l_d k_d}$	(3.6)	(3.5)	$\mathcal{O}(M^4)$
$A_{\alpha, \lambda, \kappa}$	(3.5)	(3.2)	$\mathcal{O}(M^{12})$

Table 1: The formula and computational cost to obtain  $A_{\alpha, \lambda, \kappa}$  in the VHS model and related coefficients.

**Proposition 4.** *For the Maxwell molecules, it holds for the coefficients  $A_{\alpha, \lambda, \kappa}$  that  $A_{\alpha, \lambda, \kappa} = 0$  when  $|\alpha| < |\lambda| + |\kappa|$ .*

Consequently, the eight-dimensional integral in (3.4) is reduced into merely a series of summations for the VHS model. The computational cost for all related coefficients is listed in Tab. 1. We can find that the computational cost for all  $A_{\alpha, \lambda, \kappa}$  is  $\mathcal{O}(M^{12})$ , but it will not cause much trouble since  $A_{\alpha, \lambda, \kappa}$  can be pre-computed offline and stored for the simulation. If the expansion center  $[\bar{\mathbf{u}}, \bar{\theta}]$  is chosen different from  $[\mathbf{0}, 1]$ , the coefficient  $A_{\alpha, \lambda, \kappa}^{[\bar{\mathbf{u}}, \bar{\theta}]}$  can be derived from  $A_{\alpha, \lambda, \kappa}$  through a linear transform which is stated in the proposition below.

**Proposition 5.** *In the calculation of  $A_{\alpha, \lambda, \kappa}^{[\bar{\mathbf{u}}, \bar{\theta}]}$ , we emphasize that the expansion center  $[\mathbf{0}, 1]$  is not unique. Under arbitrary expansion center  $[\bar{\mathbf{u}}, \bar{\theta}]$ , the coefficients  $A_{\alpha, \lambda, \kappa}^{[\bar{\mathbf{u}}, \bar{\theta}]}$  satisfies that*

$$A_{\alpha, \lambda, \kappa}^{[\bar{\mathbf{u}}, \bar{\theta}]} = \bar{\theta}^{1-\varpi} A_{\alpha, \lambda, \kappa}. \quad (3.18)$$

We refer the readers to [17, Sec. 3.1] for more details. Hence, we only need to compute and store  $A_{\alpha, \lambda, \kappa}$  with expansion center  $[\mathbf{0}, 1]$ .

Nevertheless, it is still quite expensive to solve the inelastic Boltzmann equation using Hermite spectral method. For example, the memory required to store  $A_{\alpha, \lambda, \kappa}$  is  $\mathcal{O}(M^9)$  [25], which is too large in practice. Moreover, the computational cost for each collision term is also  $\mathcal{O}(M^9)$ , and it will become much larger in spatially inhomogeneous tests, which is unacceptable for a large  $M$ . Thus, following the strategy in [16, 17, 25], a special design on the numerical algorithm is adopted to reduce the numerical cost, which will be introduced in the next section.

## 4 Numerical scheme

In this section, the numerical scheme to solve the moment equations (2.22) is introduced. Strang-splitting is utilized to split the moment equation into the convection step and the collision step. Precisely, the numerical scheme to solve the convection step is proposed in Sec. 4.1 and the specially designed algorithm to solve the collision step is discussed in Sec. 4.2.

For convenience, we first consider the numerical scheme for spatially one-dimensional cases, which indicates

$$\frac{\partial \cdot}{\partial x_2} = \frac{\partial \cdot}{\partial x_3} = 0. \quad (4.1)$$

Therefore, the Boltzmann equation is split into

- Convection step

$$\frac{\partial f}{\partial t} + v_1 \frac{\partial f}{\partial x_1} = 0. \quad (4.2)$$

- Collision step

$$\frac{\partial f}{\partial t} = \frac{1}{\text{Kn}} \mathcal{Q}[f, f](v). \quad (4.3)$$

#### 4.1 Convection step

Before introducing the numerical scheme to solve the convection step, we should choose the expansion center  $[\bar{u}, \bar{\theta}]$  in the expansion (2.17). Following [16, 17], spatially and temporally constant  $[\bar{u}, \bar{\theta}]$  is chosen in the convection step and the specific number is problem-dependent. Then, let  $\mathbf{f}^{[\bar{u}, \bar{\theta}]}$  be a column vector with all  $f_\alpha^{[\bar{u}, \bar{\theta}]}$ ,  $|\alpha| \leq M$  as its components. Thus, the moment equations (2.22) of the convection step can be rewritten in the matrix-vector form as

$$\frac{\partial \mathbf{f}^{[\bar{u}, \bar{\theta}]}}{\partial t} + \mathbf{A}_1^{[\bar{u}, \bar{\theta}]} \frac{\partial \mathbf{f}^{[\bar{u}, \bar{\theta}]}}{\partial x_1} = 0, \quad (4.4)$$

where  $\mathbf{A}_1^{[\bar{u}, \bar{\theta}]}$  is a constant matrix and can be diagonalized. We refer the readers to [16] for more details.

Then, we propose the numerical scheme to solve the convection term. Suppose a spatial domain  $\Omega \subset \mathbb{R}$  is discretized by a uniform grid with cell size  $\Delta x$  and cell centers  $\{x_j\}$ . We denote  $\left(\mathbf{f}_j^{[\bar{u}, \bar{\theta}]}\right)^n$  as the approximation of the average of  $\mathbf{f}^{[\bar{u}, \bar{\theta}]}$  in the  $j$ th grid cell  $[x_j - \frac{1}{2}\Delta x, x_j + \frac{1}{2}\Delta x]$  at time  $t^n$ . The finite element method is utilized to solve the convection part, and the system can be solved by the forward-Euler method with a time step size  $\Delta t$  as follows:

$$\left(\mathbf{f}^{[\bar{u}, \bar{\theta}]}\right)_j^{n+1,*} = \left(\mathbf{f}^{[\bar{u}, \bar{\theta}]}\right)_j^n - \frac{\Delta t}{\Delta x} \left(\mathbf{F}_{j+1/2}^n - \mathbf{F}_{j-1/2}^n\right), \quad (4.5)$$

where  $\mathbf{F}_{j+1/2}^n$  is the numerical flux chosen according to HLL scheme [12]

$$\mathbf{F}_{j+1/2}^n = \begin{cases} \mathbf{A}_1 \mathbf{f}_{j+1/2}^{n,L}, & \lambda^L \geq 0, \\ \frac{\lambda^R \mathbf{A}_1 \mathbf{f}_{j+1/2}^{n,L} - \lambda^L \mathbf{A}_1 \mathbf{f}_{j+1/2}^{n,R} + \lambda^R \lambda^L (\mathbf{f}_{j+1/2}^{n,R} - \mathbf{f}_{j+1/2}^{n,L})}{\lambda^R - \lambda^L}, & \lambda^L < 0 < \lambda^R, \\ \mathbf{A}_1 \mathbf{f}_{j+1/2}^{n,R}, & \lambda^R \leq 0. \end{cases} \quad (4.6)$$

where the superscript  $[\bar{u}, \bar{\theta}]$  on  $\mathbf{f}$  is omitted for neatness in (4.6).  $\lambda^L$  and  $\lambda^R$  are the characteristic velocity

$$\lambda^L = \bar{u}_1 - C_{M+1} \sqrt{\bar{\theta}}, \quad \lambda^R = \bar{u}_1 + C_{M+1} \sqrt{\bar{\theta}}, \quad (4.7)$$

which are the minimum and maximum eigenvalues of  $\mathbf{A}_1$ , and  $C_{M+1}$  is the largest root of the Hermite polynomial of degree  $M + 1$ . In (4.6),  $\mathbf{f}_{j+1/2}^{n,L}$  and  $\mathbf{f}_{j+1/2}^{n,R}$  are computed with WENO reconstruction [20], and the details are given in App. D. In addition, the time step size must be chosen to satisfy the CFL condition

$$\text{CFL} \triangleq \Delta t \frac{|\bar{u}_1| + C_{M+1} \sqrt{\bar{\theta}}}{\Delta x} < 1. \quad (4.8)$$

Now we complete the numerical scheme of spatially one-dimensional case. This scheme can be naturally extended to spatially three-dimensional situations.

## 4.2 Collision step

For the collision step, as is stated, the computational cost to compute the collision term is still quite expensive as  $\mathcal{O}(M^9)$ . Therefore, a new collision model is built to reduce cost following the idea in [25]. Here, we will introduce the new collision model, and then introduce the numerical scheme in the collision step.

### 4.2.1 Building new collision model

To build the new collision model, the quadratic collision term and a simplified operator such as the BGK operator are combined, where the quadratic operator is utilized to deal with the low-order terms in the new collision model, while the high-order terms will be approximated with the simplified collision operator to save memory and computational cost. In the inelastic case, the linear model with a similar form to (2.10) is utilized as

$$\mathcal{Q}_L[f](\mathbf{v}) = \nu_1 \rho [f_G(\mathbf{v}) - f(\mathbf{v})] + \nu_2 \rho \nabla_{\mathbf{v}} \cdot [(\mathbf{v} - \mathbf{u})f(\mathbf{v})]. \quad (4.9)$$

Different from (2.10), there is a  $\rho$  here in each term to match the quadratic form of distribution functions in the original collision model.  $\nu_1$  and  $\nu_2$  are some constant parameters, which will be discussed later.

We first discuss the Hermite expansion of  $\mathcal{Q}_L(\mathbf{v})$ . Same as the BGK operator in the classical case [16, 17], the expansion center is chosen as the local macroscopic velocity and temperature as

$$f(t, \mathbf{x}, \mathbf{v}) \approx \sum_{|\alpha| \leq M} f_{\alpha}^{[\mathbf{u}, \theta]}(t, \mathbf{x}) \mathcal{H}_{\alpha}^{[\mathbf{u}, \theta]}(\mathbf{v}), \quad (4.10)$$

with which the computational cost for expanding the collision term (4.9) can be greatly reduced. Thus, the expansion coefficients of  $f_G$  can be computed with [6]

$$f_{G, \alpha}^{[\mathbf{u}, \theta]} = \begin{cases} \rho, & \alpha = 0, \\ 0, & |\alpha| = 1, \\ \frac{1 - 1/\text{Pr}}{\alpha_i \rho} \sum_{k=1}^3 \sigma_{ik} f_{G, \alpha - e_i - e_k}^{[\mathbf{u}, \theta]}, & |\alpha| \geq 2, i \in \{1, 2, 3\} \text{ s.t. } \alpha_i > 0. \end{cases} \quad (4.11)$$

Here we emphasize that the last relationship in (4.11) holds for any  $i \in \{1, 2, 3\}$  subject to  $\alpha_i > 0$ . With  $f_0^{[\mathbf{u}, \theta]} = \rho$ , the energy loss term  $\rho \nabla_{\mathbf{v}} \cdot [(\mathbf{v} - \mathbf{u})f(\mathbf{v})]$  is expanded as

$$\rho \nabla_{\mathbf{v}} \cdot [(\mathbf{v} - \mathbf{u})f(\mathbf{v})] \approx \sum_{|\alpha| \leq M} f_0^{[\mathbf{u}, \theta]} \left( |\alpha| f_{\alpha}^{[\mathbf{u}, \theta]} + \sum_{d=1}^3 f_{\alpha - 2e_d}^{[\mathbf{u}, \theta]} \right) \mathcal{H}_{\alpha}^{[\mathbf{u}, \theta]}(\mathbf{v}), \quad (4.12)$$

where  $f_{\alpha}^{[\mathbf{u}, \theta]}$  is regarded as 0 in (4.11) and (4.12) if  $\alpha$  contains any negative index. let  $\mathbf{f}^{[\mathbf{u}, \theta]}$  be a column vector with all  $f_{\alpha}^{[\mathbf{u}, \theta]}, |\alpha| \leq M$  as its components. Combining (4.11) and (4.12), the linear collision model  $\mathcal{Q}_L(\mathbf{v})$  can be expanded as

$$\mathcal{Q}_L[f](\mathbf{v}) \approx \sum_{|\alpha| \leq M} \mathcal{Q}_{L, \alpha}[\mathbf{f}^{[\mathbf{u}, \theta]}] \mathcal{H}_{\alpha}^{[\mathbf{u}, \theta]}(\mathbf{v}), \quad (4.13)$$

with

$$\mathcal{Q}_{L, \alpha}[\mathbf{f}^{[\mathbf{u}, \theta]}] = \nu_1 f_0^{[\mathbf{u}, \theta]} \left( f_{G, \alpha}^{[\mathbf{u}, \theta]} - f_{\alpha}^{[\mathbf{u}, \theta]} \right) - \nu_2 f_0^{[\mathbf{u}, \theta]} \left( |\alpha| f_{\alpha}^{[\mathbf{u}, \theta]} + \sum_{d=1}^3 f_{\alpha - 2e_d}^{[\mathbf{u}, \theta]} \right). \quad (4.14)$$

Next, following similar lines in [17, 25], we will build the new collision model that is combined with the quadratic collision term (2.21) and linearized operator (4.13) as

$$\mathcal{Q}_{\text{new}}[f](v) = \sum_{|\alpha| \leq M} Q_{\text{new}, \alpha}[\mathbf{f}^{[u, \theta]}, \mathbf{f}^{[u, \theta]}] \mathcal{H}_{\alpha}^{[u, \theta]}(v), \quad (4.15)$$

with

$$Q_{\text{new}, \alpha}[\mathbf{f}^{[u, \theta]}, \mathbf{f}^{[u, \theta]}] = \begin{cases} \sum_{|\lambda|, |\kappa| \leq M_0} A_{\alpha, \lambda, \kappa}^{[u, \theta]} f_{\lambda}^{[u, \theta]} f_{\kappa}^{[u, \theta]}, & |\alpha| \leq M_0, \\ Q_{L, \alpha}[\mathbf{f}^{[u, \theta]}], & M_0 < |\alpha| \leq M. \end{cases} \quad (4.16)$$

**Remark 1.** In (4.16), the coefficient  $A_{\alpha, \lambda, \kappa}^{[u, \theta]}$  is derived through  $A_{\alpha, \lambda, \kappa}$  with Proposition 5. The parameter  $M_0$  is problem-dependent, which is always decided empirically. Based on our experience,  $M_0 = 10$  is enough for most problems.

Then let us go back to (4.14) and decide the parameters  $\nu_1$  and  $\nu_2$  to complete the collision model. Since  $\nu_1$  indicates the damping rate of high-order terms, we follow the same idea in [25, Sec. 3.3.2] to decide this parameter, where it is expected that the high-order terms decay faster but do not introduce any gap in the damping rate between the terms of  $|\alpha| \leq M_0$  and  $|\alpha| > M_0$ . Thus,  $A_{\alpha, \lambda, \kappa}$  is regarded as a matrix with respect to  $\lambda$  and  $\kappa$  for each fixed  $\alpha$ , and  $\nu_1$  is set to be the minimum of all eigenvalues of  $A_{\alpha, \lambda, \kappa}$  among  $|\alpha| \leq M_0$  (i.e. the spectral radius of damping rate in quadratic part). We refer the readers to [25, Sec. 3.3.2] for more details. As to  $\nu_2$ , it is borrowed from the cooling rate in [2, (2.16)] that

$$\nu_2 = \frac{2}{3\sqrt{\pi}}(1 - e^2). \quad (4.17)$$

So far, we have derived the new collision model. The numerical scheme to solve the collision step using this new collision model is discussed in the next section.

#### 4.2.2 Numerical scheme to update the collision step

Based on the new collision model, the numerical scheme to update the collision step is presented in this section. In the framework of the Hermite spectral method, the governing equation in the collision step (4.3) is reduced into

$$\frac{\partial \mathbf{f}_j^{[u, \theta]}}{\partial t} = \frac{1}{\text{Kn}} \mathbf{Q}_{\text{new}}[\mathbf{f}^{[u, \theta]}, \mathbf{f}^{[u, \theta]}], \quad (4.18)$$

where  $\mathbf{Q}_{\text{new}}[\mathbf{f}^{[u, \theta]}, \mathbf{f}^{[u, \theta]}]$  is a column vector with all  $Q_{\text{new}, \alpha}[\mathbf{f}^{[u, \theta]}, \mathbf{f}^{[u, \theta]}]$ ,  $|\alpha| \leq M$  as its components. After the convection step at time  $t^{n+1}$ ,  $\left(\mathbf{f}^{[\bar{u}, \bar{\theta}]}\right)_j^{n+1, *}$  is obtained. Then we derive the expansion coefficients  $\left(\mathbf{f}^{[u_j^{n+1, *}, \theta_j^{n+1, *}]} \right)_j^{n+1, *}$  under the expansion center  $[u_j^{n+1, *}, \theta_j^{n+1, *}]$  with the projection algorithm in Theorem 6. The expansion center  $[u_j^{n+1, *}, \theta_j^{n+1, *}]$  is the macroscopic velocity and temperature after the convection step at time  $t^{n+1}$ , which is obtained by (2.19). Next, the forward Euler scheme is adopted to update (4.18) as

$$(\mathbf{f}^*)_j^{n+1} = (\mathbf{f}^*)_j^{n+1, *} + \Delta t \mathbf{Q}_{\text{new}} \left[ (\mathbf{f}^*)_j^{n+1, *}, (\mathbf{f}^*)_j^{n+1, *} \right], \quad (4.19)$$

where  $\mathbf{f}^* \triangleq \mathbf{f}^{[u_j^{n+1, *}, \theta_j^{n+1, *}]}$  for abbreviation. Finally, the projection algorithm in Theorem 6 is utilized once again to obtain  $\left(\mathbf{f}^{[\bar{u}, \bar{\theta}]}\right)_j^{n+1}$  based on  $(\mathbf{f}^*)_j^{n+1}$ , which finishes the collision part and enters the next time step.

### 4.3 Outline of the numerical algorithm

The overall numerical scheme is summarized in Algorithm 1.

---

**Algorithm 1** Numerical algorithm

---

- 1: Preparation: calculate and store  $A_{\alpha,\lambda,\kappa}$  in (3.4) with the algorithm in Sec. 3.
  - 2: Let  $n = 0$ , and determine an expansion center  $[\bar{\mathbf{u}}, \bar{\theta}]$  for the convection step. Calculate the initial value of  $\left(\mathbf{f}^{[\bar{\mathbf{u}}, \bar{\theta}]}\right)_j^0$ .
  - 3: Set the time step  $\Delta t^n$  with the CFL condition (4.8).
  - 4: Solve the convection step (4.5) to obtain  $\left(\mathbf{f}^{[\bar{\mathbf{u}}, \bar{\theta}]}\right)_j^{n+1,*}$ .
  - 5: Obtain the macroscopic velocity and temperature  $\mathbf{u}_j^{n+1,*}, \theta_j^{n+1,*}$  of  $\left(\mathbf{f}^{[\bar{\mathbf{u}}, \bar{\theta}]}\right)_j^{n+1,*}$  using (2.19).
  - 6: Project  $\left(\mathbf{f}^{[\bar{\mathbf{u}}, \bar{\theta}]}\right)_j^{n+1,*}$  to the function space of expansion center  $[\mathbf{u}_j^{n+1,*}, \theta_j^{n+1,*}]$  with Theorem 6, and obtain  $\left(\mathbf{f}^{[\mathbf{u}_j^{n+1,*}, \theta_j^{n+1,*}]}\right)_j^{n+1,*}$ .
  - 7: Update  $\left(\mathbf{f}^{[\mathbf{u}_j^{n+1,*}, \theta_j^{n+1,*}]}\right)_j^{n+1}$  with (4.19).
  - 8: Project  $\left(\mathbf{f}^{[\mathbf{u}_j^{n+1,*}, \theta_j^{n+1,*}]}\right)_j^{n+1}$  to the function space of expansion center  $[\bar{\mathbf{u}}, \bar{\theta}]$ , and obtain  $\left(\mathbf{f}^{[\bar{\mathbf{u}}, \bar{\theta}]}\right)_j^{n+1}$ .
  - 9: Let  $n \leftarrow n + 1$ , and return to step 3.
- 

## 5 Numerical experiments

In this section, several numerical experiments are carried out to validate this Hermite spectral method for the inelastic Boltzmann equation. Firstly, two homogeneous cases will be tested for Maxwell molecules and hard sphere (HS) collision kernel. Next, two spatially one-dimensional problems and a spatially two-dimensional problem will be studied with the HS collision kernel.

### 5.1 Homogeneous experiments

In this section, two homogeneous problems, the heating source problem, and Haff's cooling law are studied, where the Maxwell molecular model is adopted in the heating source problem, and the HS model is utilized in Haff's cooling law.

#### 5.1.1 Heating source problem

In this section, the heating source problem is studied, which is first introduced in [23], and similar studies can also be found in [8, 26]. Its governing equation is

$$\frac{\partial f}{\partial t} - \varepsilon \Delta_v f = \frac{1}{\text{Kn}} \mathcal{Q}[f, f](\mathbf{v}), \quad (5.1)$$

where the second term represents the effect of the heating source with the diffusion coefficient  $\varepsilon \ll 1$ . In this test, the Maxwell molecular model is utilized, and the Knudsen number is chosen

such that  $\frac{1}{\text{Kn}}B = \frac{1}{4\pi}$ . First, taking  $\phi = 1, \mathbf{v}$  in (2.8), the conservation of mass and momentum can be derived as

$$\rho \equiv \rho_0, \quad \mathbf{u} = \mathbf{u}_0, \quad (5.2)$$

where  $\rho_0$  and  $\mathbf{u}_0$  are the initial density and macroscopic velocity, respectively. Without loss of generality, we let  $\rho_0 \equiv 1$  and  $\mathbf{u}_0 \equiv \mathbf{0}$ . Moreover, multiplying  $\phi = |\mathbf{v}|^2/3$  on both sides of (5.1) and using the weak form in (2.8), we can derive the governing equation of the temperature  $\theta$  as [8]

$$\frac{\partial \theta}{\partial t} - 2\varepsilon \rho_0 = -\frac{1-e^2}{4}\theta, \quad (5.3)$$

whose exact solution is

$$\theta(t) = \left( \theta(0) - \frac{8\varepsilon}{1-e^2} \right) \exp\left(-\frac{1-e^2}{4}t\right) + \frac{8\varepsilon}{1-e^2}. \quad (5.4)$$

In the numerical simulation, the expansion center is selected as  $[\bar{\mathbf{u}}, \bar{\theta}] = [\mathbf{0}, 1]$ , then the moment system of (5.1) is derived as

$$\frac{df_\alpha}{dt} - \varepsilon \sum_{d=1}^3 f_{\alpha-2e_d} = Q_{\text{new},\alpha}, \quad |\alpha| \leq M, \quad (5.5)$$

where  $Q_{\text{new},\alpha}$  is obtained in (4.16).

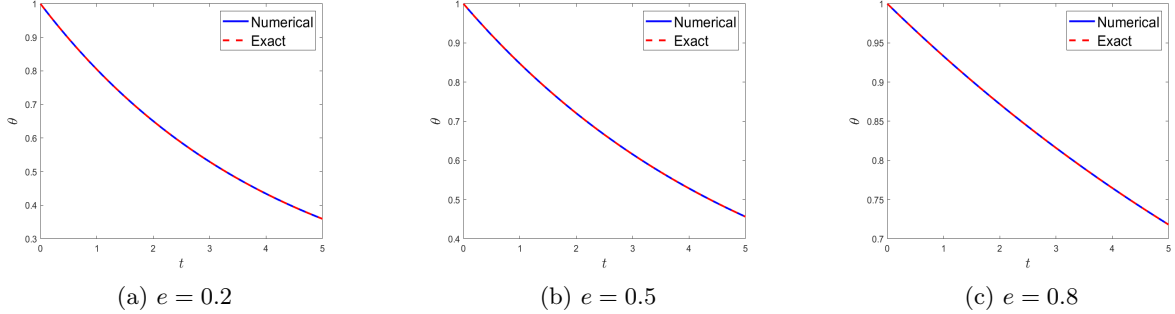


Figure 1: (Heating Problem in Sec. 5.1.1) Evolution of temperature in the heating source problem. The restitution coefficients are  $e = 0.2, 0.5$  and  $0.8$ , successively. The blue line is the numerical solution, while the red line is the exact solution in (5.4).

Since there is no analytical solution to this heating source problem, the solution of temperature always serves as the reference solution in this numerical test. In the simulation, the parameter  $\varepsilon$  is set as  $\varepsilon = 0.01$ , and the initial condition is

$$f(0, \mathbf{v}) = \mathcal{M}_{0,1}(\mathbf{v}) = \frac{1}{(2\pi)^{3/2}} \exp\left(-\frac{|\mathbf{v}|^2}{2}\right). \quad (5.6)$$

Thus, the initial condition for temperature  $\theta$  is  $\theta(0) = 1$ . Moreover, the length of the quadratic collision and the total expansion order are chosen as  $[M_0, M] = [10, 10]$ . The restitution coefficient  $e = 0.2, 0.5, 0.8$  from  $t = 0$  to  $t = 5$  are tested, and the time step length is  $\Delta t = 0.01$ . The evolution of temperature  $\theta$  is displayed in Fig. 1, which implies that the numerical solution matches well with the analytical solution for the temperature.

**Remark 2.** Here, we want to emphasize that as is shown in Proposition 4, the coefficients  $A_{\alpha,\lambda,\kappa}$  can be nonzero only when  $|\alpha| \geq |\kappa| + |\lambda|$ . Thus, (5.5) is naturally closed for any  $M_0$  and  $M$ . That is to say, the higher-order moments will not affect the lower-order ones through the collision term, and  $\theta$  can be represented by  $M = 2$ . Therefore, we can obtain the evolution of temperature  $\theta$  through the moment system (5.5) with  $[M_0, M] = [2, 2]$ , and the computational cost can be greatly reduced.

### 5.1.2 Haff's cooling law

In this section, we will try to observe Haff's cooling law numerically, which is first proposed by Haff in [11]. The governing equation for Haff's cooling law is the same as the heating source problem as (5.1) with  $\epsilon = 0$ . Haff's law implies that for the gas composed of inelastic hard spheres, the temperature in the spatially homogeneous problem will evolve as

$$\theta(t) \approx \frac{\theta(0)}{(1 + \gamma_0 t)^2}. \quad (5.7)$$

Different from the Maxwell molecules, the decay speed here is  $\mathcal{O}(t^{-2})$ . Here  $\gamma_0$  is a positive constant depending on the value of  $e$ . We refer [7, 14] for more details of this numerical test. The nondimensionalized HS collision model has the form

$$B = \frac{1}{4\sqrt{2}\pi} |g|. \quad (5.8)$$

Meanwhile, the same initial condition as (5.6) is adopted, and the Knudsen number is set to be  $\text{Kn} = 1/\sqrt{e}$ . The length of the quadratic collision and the total expansion order are chosen as  $[M_0, M] = [10, 40]$ , and the time step length is  $\Delta t = 0.01$ . The evolution of the temperature with  $e = 0.2, 0.5, 0.8$  from  $t = 0$  to  $t = 5$  is shown in Fig. 2, where the reference solution is derived by estimating  $\gamma_0$  in (5.7) with the least square fitting. From Fig. 2, it can be clearly seen that even in the case  $e = 0.2$ , the numerical solution matches well with the reference solution. Besides, we want to emphasize that Proposition 4 does not hold for the HS collision model, therefore the expansion number can not be set as  $[2, 2]$  to capture the evolution of temperature.

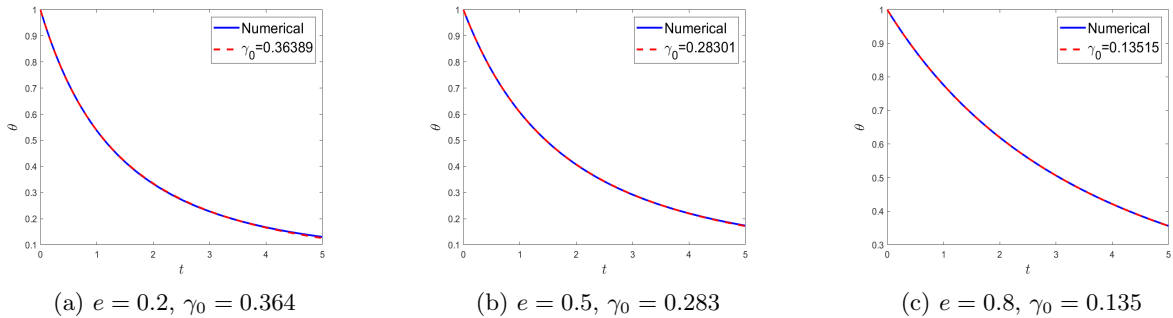


Figure 2: (Haff's cooling law in Sec. 5.1.2) Time evolution of temperature in Haff's cooling law. The restitution coefficients are  $e = 0.2, 0.5$  and  $0.8$ , successively. The blue line is the numerical solution, and the red line is the reference solution.

## 5.2 Inhomogeneous experiments

In this section, two spatially one-dimensional problems, the Couette flow and Fourier heat transfer, and one spatially two-dimensional problem the periodic diffusion are studied. In all the tests, Argon is taken as the working gas, and the HS model is utilized as the collision model. The Knudsen number is calculated with

$$\text{Kn} = \frac{m_0}{\sqrt{2}\pi\rho_0 d_{\text{ref}}^2 x_0}. \quad (5.9)$$

Here, the parameters in (5.9) are the nondimensionalization parameters of Argon and HS collision kernel, which are shown in Tab. 3, with the method of nondimensionalization listed in App. E. The DSMC method provided in [2] for the HS collision kernel is utilized to provide the reference solution.

### 5.2.1 Couette flow

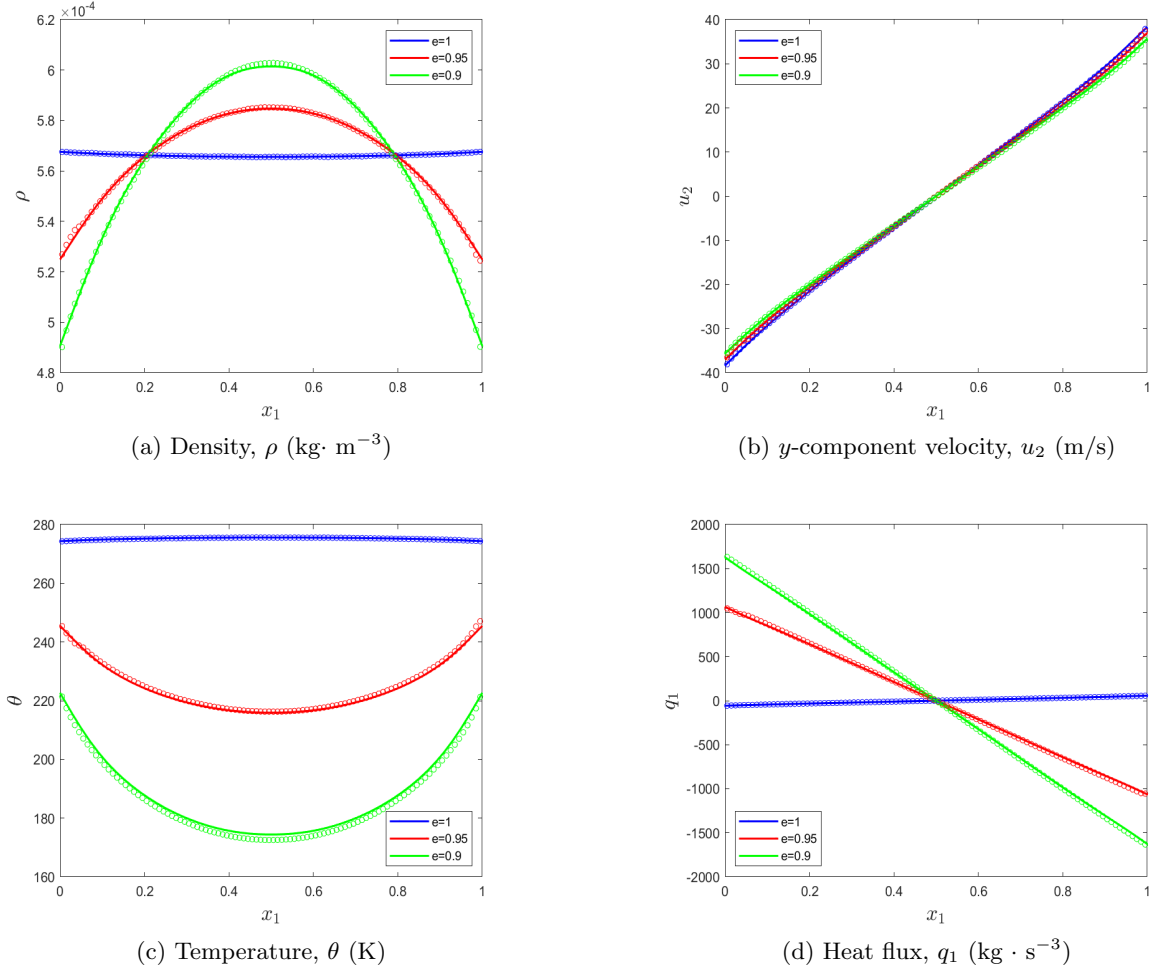


Figure 3: (Couette flow in Sec. 5.2.1): Numerical solution of the Couette flow for  $\text{Kn} = 0.2$  with  $e = 1, 0.95$  and  $0.9$ . Lines correspond to numerical solutions and symbols denote the reference solutions from DSMC.



In this section, we will consider the 1D Couette flow, which is a benchmark problem also tested in [16, 26]. There are two infinite parallel plates with a distance of  $10^{-3}$  m. Both plates are purely diffusive and have a temperature of 273K. They move in the opposite direction along with the plate with the speed  $\mathbf{u}^w = (0, \mp 50, 0)$  m/s. Argon is filled in these two plates with velocity  $\mathbf{u} = 0$  m/s, and temperature  $\theta = 273$  K. Two densities are considered as  $\rho = 5.662 \times 10^{-4} \text{ kg} \cdot \text{m}^{-3}$  and  $1.132 \times 10^{-4} \text{ kg} \cdot \text{m}^{-3}$ , which correspond to  $\text{Kn} = 0.2$  and 1 respectively.

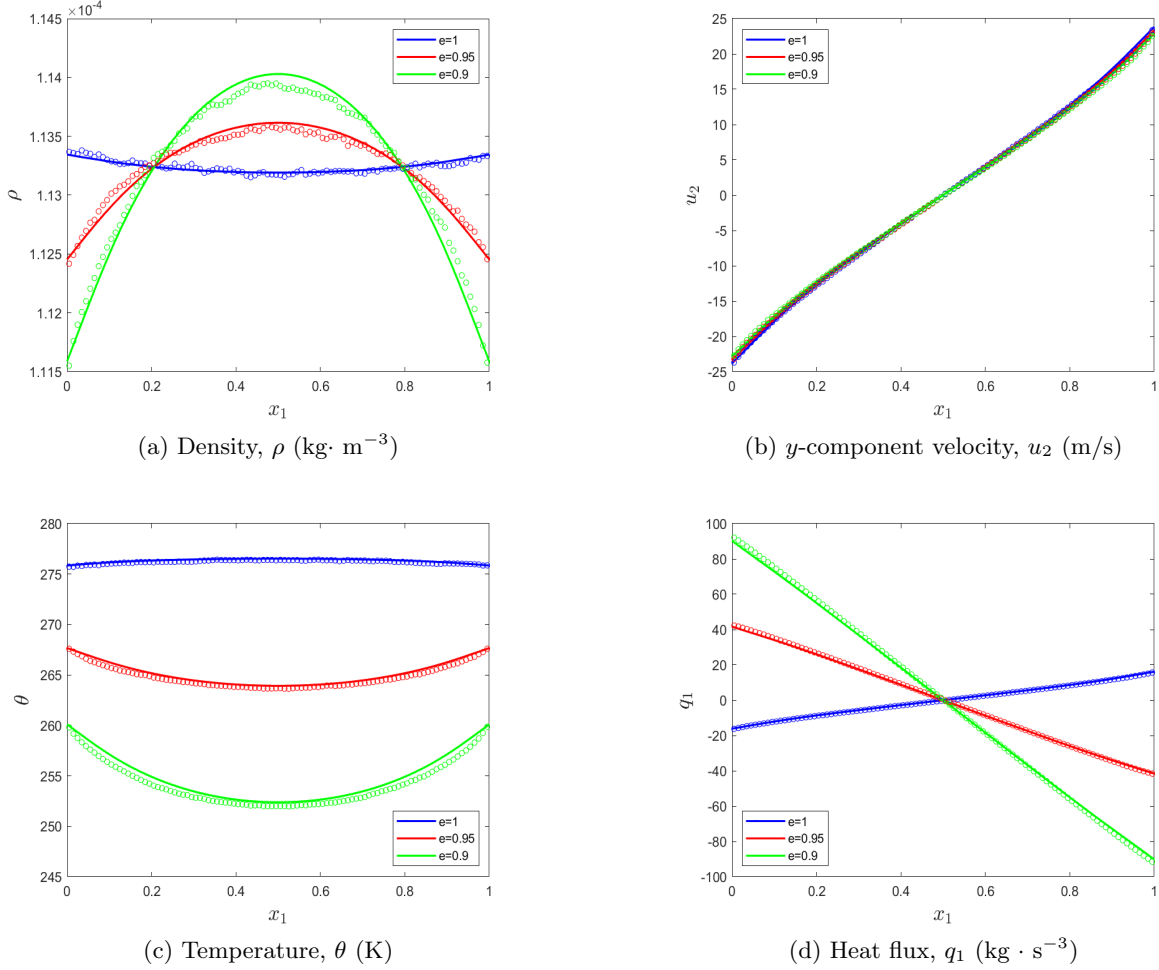


Figure 4: (Couette flow in Sec. 5.2.1) Numerical solution of the Couette flow for  $\text{Kn} = 1.0$  with  $e = 1, 0.95$  and  $0.9$ . Lines correspond to numerical solutions and symbols denote the reference solutions from DSMC.

In the simulation, a uniform grid with 50 cells and WENO reconstruction is utilized for the spatial discretization and the CFL condition number is set as  $\text{CFL} = 0.3$ . The length for the quadratic collision term and the total expansion number are chosen as  $[M_0, M] = [10, 40]$ . The expansion center  $[\bar{\mathbf{u}}, \bar{\theta}]$  in the convection step is  $[0, 1]$  and the restitution coefficients  $e = 1, 0.95$ , and  $0.9$  are implemented. The density  $\rho$ , macroscopic velocity in the  $y$ -direction  $u_2$ , temperature  $\theta$ , and the heat flux  $q_1$  in the  $x$ -direction at the steady state are studied, and the numerical results for  $\text{Kn} = 0.2$  and 1 are illustrated in Fig. 3 and 4, respectively. When  $\text{Kn} = 0.2$ , all the numerical solutions coincide well with the reference solution. For the case  $\text{Kn} = 1$ , the velocity  $u_2$ , temperature  $\theta$  and heat flux  $q_1$  agree well with the reference solution, while there is a small

discrepancy in the density  $\rho$ , but the largest relative error is less than 1%. We also want to emphasize that there are some oscillations in the reference results, while the numerical solution keeps smooth.

### 5.2.2 Fourier heat transfer

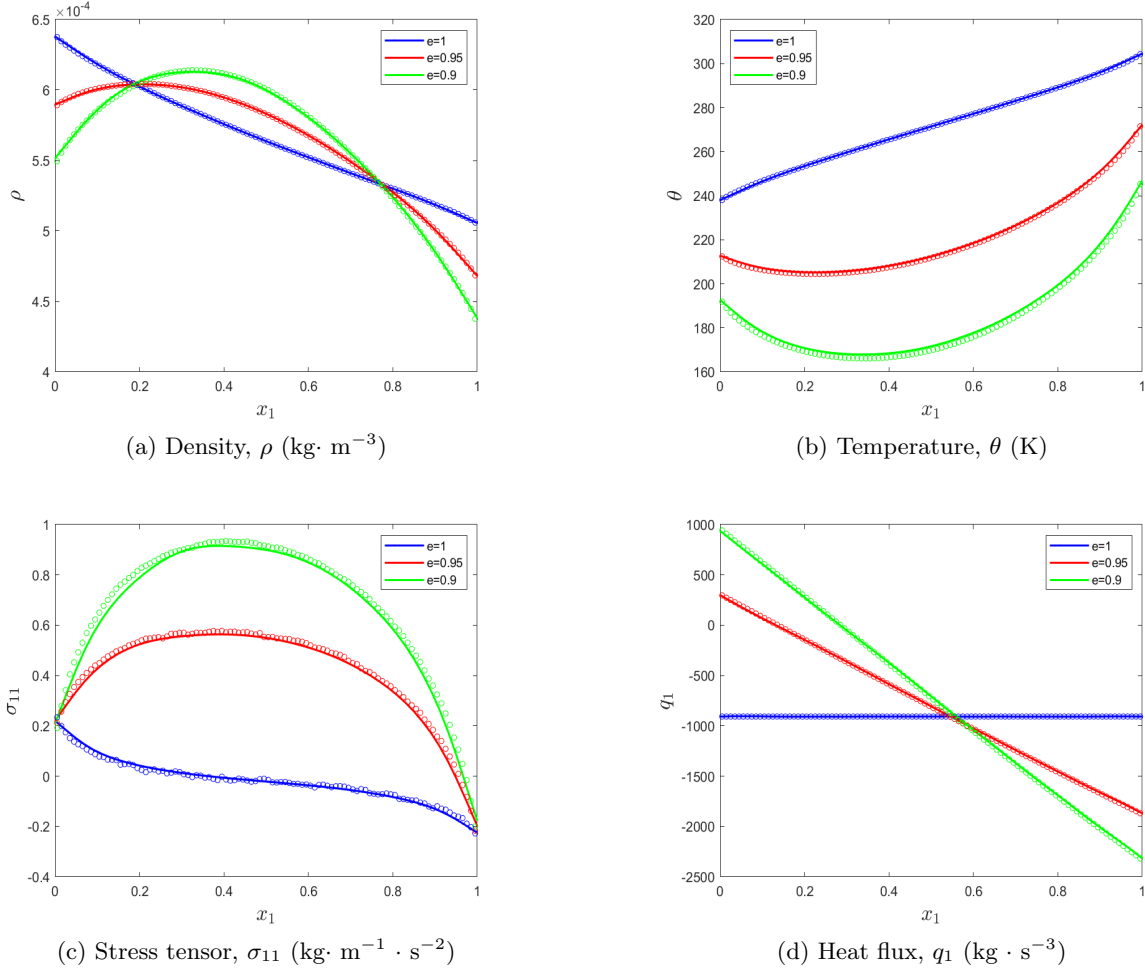


Figure 5: (Fourier heat transfer in Sec. 5.2.2) Numerical solutions of the Fourier flow for  $\text{Kn} = 0.2$  with  $e = 1, 0.95$  and  $0.9$ . Lines correspond to numerical solutions and symbols denote the reference solutions from DSMC.

Fourier heat transfer is another widely studied problem in kinetic theory, which is also considered in [26]. Similar to the Couette flow, we consider the gas of Argon between two infinitely large parallel plates. The distance between the plates is still  $10^{-3}\text{m}$  and both boundaries are purely diffusive. Different from Couette flow, the two plates are stationary but have a distinction in temperature. Here, the temperatures of two walls are set as  $\theta_l = 223\text{K}$  and  $\theta_r = 323\text{K}$ . The initial condition for Argon is velocity  $\mathbf{u} = \mathbf{0}\text{m/s}$ , and temperature  $\theta = 273\text{K}$ . Two densities are considered as  $\rho = 5.662 \times 10^{-4}\text{kg} \cdot \text{m}^{-3}$  and  $1.132 \times 10^{-4}\text{kg} \cdot \text{m}^{-3}$ , which correspond to  $\text{Kn} = 0.2$  and 1 respectively.

The same numerical setting such as grid, CFL number, expansion center, etc. as the Couette

flow 5.2.1 is utilized. The numerical results for  $\text{Kn} = 0.2$  and 1 are plotted in Fig. 5, and 6, respectively, where the density  $\rho$ , temperature  $\theta$ , the shear stress  $\sigma_{11}$ , and heat flux  $q_1$  are illustrated. We can find for both  $\text{Kn}$ , the numerical solution match well with the reference, and the largest relative deviation is less than 0.5% in all cases. Besides, different from the reference solution by DSMC, the numerical results keep smooth.

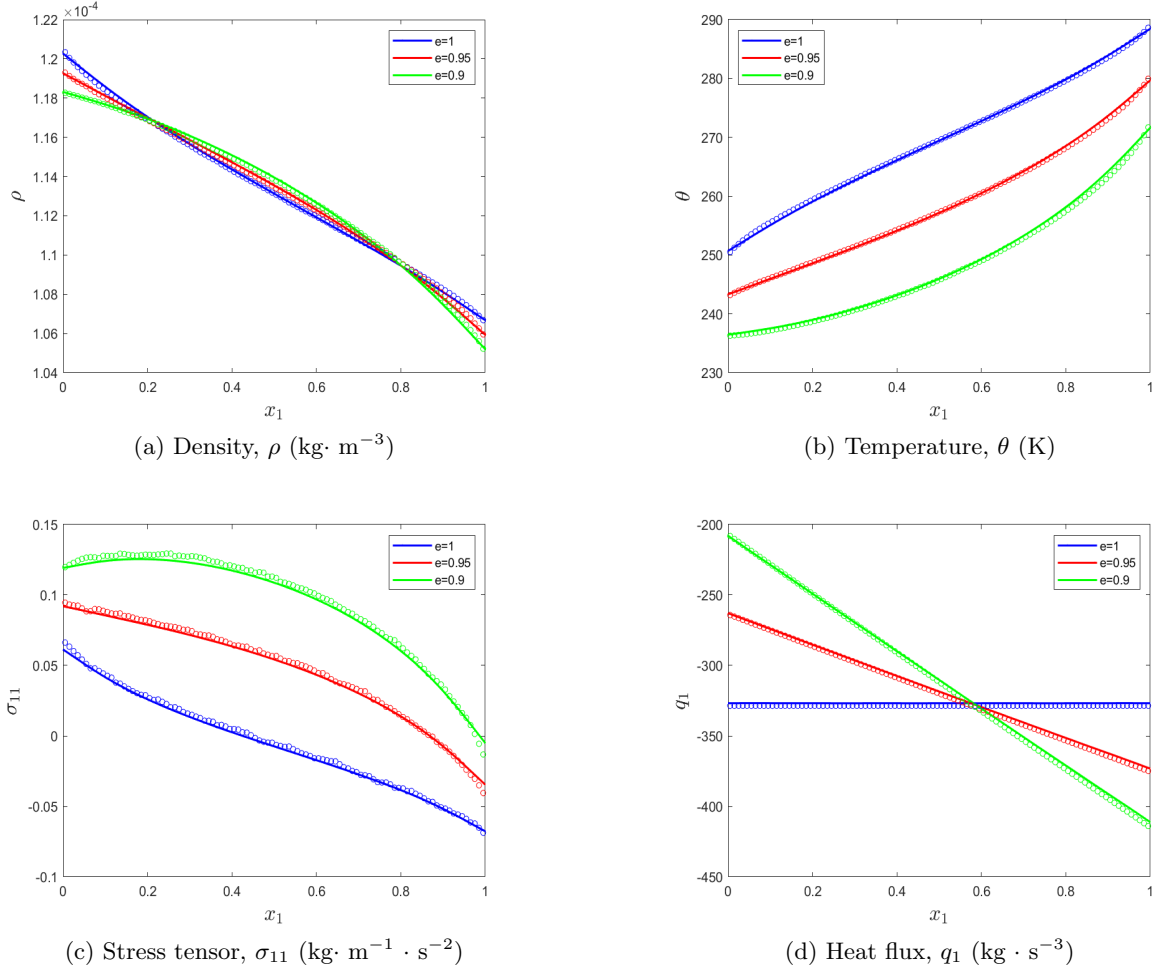


Figure 6: (Fourier flow in Sec. 5.2.2) Numerical solutions of the Fourier flow for  $\text{Kn} = 1.0$  with  $e = 1, 0.95$  and  $0.9$ . Lines correspond to numerical solutions and symbols denote the reference solutions from DSMC.

### 5.2.3 2D case: periodic diffusion

In this section, we consider a two-dimensional test with periodic boundary conditions. Argon is also taken as the working gas in the square region  $\Omega = [0, L] \times [0, L]$ , where  $L = 10^{-3}\text{m}$ . To validate the efficiency of this Hermite method, two examples with different initial conditions are tested.

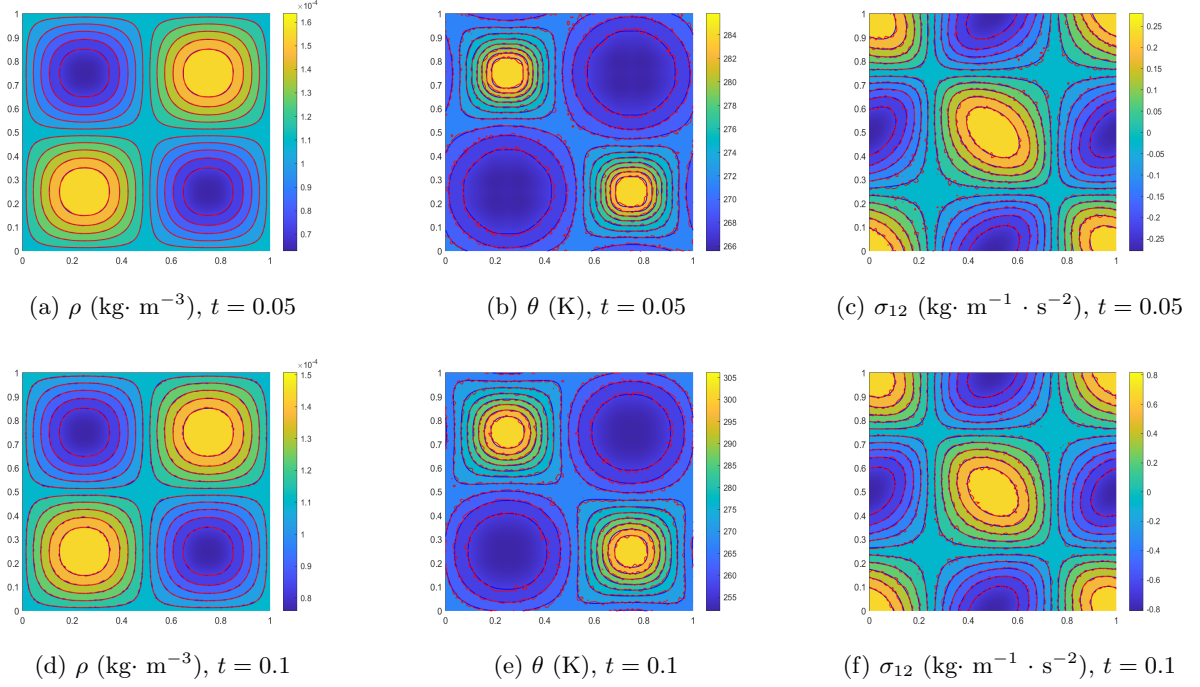


Figure 7: (2D case: periodic diffusion in Sec. 5.2.3, Example 1) Solution of the periodic diffusion for  $e = 0.9$  with the initial condition (5.10). Blue contours: Numerical solution. Red contours: Reference solution by DSMC.

**Example 1** In the first example, the initial velocity and temperature are set as  $\mathbf{u} = \mathbf{0}$  and  $\theta = 273\text{K}$  in the whole area, while the initial density  $\rho(x, y)$  is

$$\rho(x, y) = 1.132 \times 10^{-4} \times \left[ 1 + 0.5 \sin\left(2\pi \frac{x}{L}\right) \sin\left(2\pi \frac{y}{L}\right) \right] \text{kg} \cdot \text{m}^{-3}. \quad (5.10)$$

In the classical case, the distribution function will diffuse to reach global equilibrium. From the macroscopic view, the macroscopic variables will finally be spatially uniform. However, in the inelastic case, due to the dissipation of total energy, the evolution of non-equilibrium macroscopic variables, especially temperature, will become much more complicated, and will approach zero with time increasing.

In the simulation, a uniform grid with  $100 \times 100$  cells and WENO reconstruction is adopted for spatial discretization. With this initial condition, the corresponding Knudsen number is  $\text{Kn} = 1$ . The quadratic length and total expansion number are set as  $[M_0, M] = [10, 30]$ . The expansion center for the convection step is  $[\bar{\mathbf{u}}, \bar{\theta}] = [\mathbf{0}, 1]$ .

The restitution coefficient  $e = 0.9$  is implemented in the simulation. The macroscopic variables such as the density  $\rho$ , the temperature  $\theta$ , and the stress tensor  $\sigma_{12}$  are studied. The numerical results are illustrated in Fig. 7, where the solution by DSMC is utilized as the reference solution. We can see that the numerical solution coincides well with the reference solution. Moreover, there are some oscillations in the reference solution, while the numerical solution keeps smooth.

**Example 2** To further validate the efficiency of this method, a more complicated initial condition is studied, where the variation period for the density is smaller, and some disturbance is

added in the temperature as

$$\begin{aligned}\rho(x, y) &= 1.132 \times 10^{-4} \times \left[ 1 + 0.5 \sin\left(2\pi \frac{x}{L}\right) \sin\left(4\pi \frac{y}{L}\right) \right] \text{ kg} \cdot \text{m}^{-3}, \\ \theta(x, y) &= 273 \times \left[ 1 + 0.05 \sin\left(2\pi \frac{x}{L}\right) \sin\left(2\pi \frac{y}{L}\right) \right] \text{ K}.\end{aligned}\tag{5.11}$$

The numerical settings here such as the mesh, expansion order, et al. are the same as **Example 1**, but a smaller restitution coefficient  $e = 0.8$  is studied. The numerical solution of the density  $\rho$ , the temperature  $\theta$ , and the stress tensor  $\sigma_{12}$  at  $t = 0.05$  and  $t = 0.1$  is plotted in Fig. 8. We can see that for this complex initial condition, the numerical solutions still agree well with the reference solution. The variation trend of these macroscopic variables is also similar to **Example 1**, while the behavior of the temperature seems more complicated.

To explore a longer behavior of this example, the numerical solution at  $t = 0.2$  is displayed in Fig. 9, where we find that these three macroscopic variables are becoming spatially uniform, and the temperature is globally decreasing. We want to emphasize that the reference solution by DSMC is filled with oscillations, which can not describe this behavior of the example with a longer time, while the numerical solution of the Hermite spectral method is still smooth.

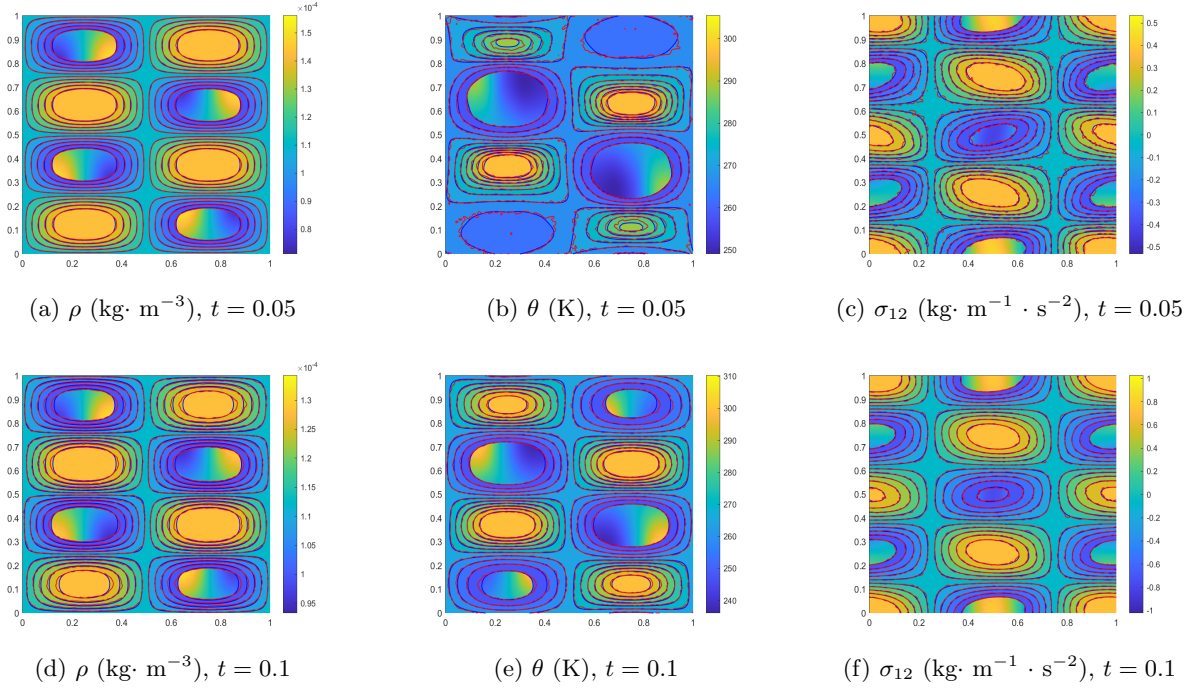


Figure 8: (2D case: periodic diffusion in Sec. 5.2.3, Example 2) Solution of the periodic diffusion for  $e = 0.8$  with the initial condition (5.11). Blue contours: Numerical solution. Red contours: Reference solution by DSMC.

**Efficiency test** To show the efficiency of this method quantitatively, the computational time for these two examples is studied. The simulations are done on the CPU model Intel Xeon E5-2697A V4 @ 2.6GHz, and 8 threads are utilized. The total CPU time and wall time, as well as the CPU time of each time step and each grid, are provided in Tab. 2. It shows that the total time for  $e = 0.9$  and  $e = 0.8$  is almost the same, which indicates that the effect of the

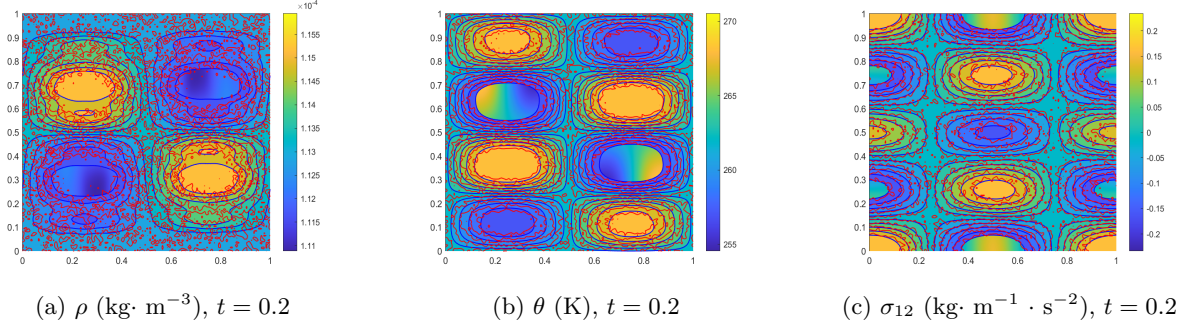


Figure 9: (2D case: periodic diffusion in Sec. 5.2.3, Example 2) Solution of the periodic diffusion for  $e = 0.8$  with the initial condition (5.11) at  $t = 0.2$ . Blue contours: Numerical solution. Red contours: Reference solution by DSMC.

restitution coefficient on the computational time is almost negligible. Moreover, the total CPU time is almost 8 times of the elapsed time, which indicates the amazing parallel efficiency of this Hermite spectral method. Besides, the total degrees of freedom (DOF) in the microscopic velocity space is

$$\text{DOF} = \frac{(M+2)(M+1)M}{6}. \quad (5.12)$$

Then, the total DOF in this 2D problem is 4960 and the CPU time per DOF per grid given in Tab. 2 is at  $\mathcal{O}(10^{-6})$ . All these results reveal the high efficiency of this Hermite spectral method, and it will work well with parallel computing in large-scale problems.

	Example 1	Example 2
$[M_0, M]$	[10, 30]	[10, 30]
Restitution coefficient $e$	0.9	0.8
End time $t$	0.1	0.1
Run-time data:		
Total CPU time $T_{\text{CPU}}$ (s):	79980	81454
Elapsed time (Wall time) $T_{\text{Wall}}$ (s):	10575.8	10856.3
Parallel efficiency:	94.53%	93.79%
CPU time per time step (s):	242.36	246.83
Degree of freedom	4960	4960
CPU time per DOF per grid (s)	$4.9 \times 10^{-6}$	$5.0 \times 10^{-6}$

Table 2: (2D case: periodic diffusion in Sec. 5.2.3) Run-time data for two-dimensional periodic diffusion of  $t = 0.1$ .

## 6 Conclusion

In this paper, we have developed a numerical scheme of the inelastic Boltzmann equation based on the Hermite spectral method, which makes us even capable to compute two-dimensional periodic model problems. The expansion coefficients of the quadratic collision model are computed



utilizing the properties of the Hermite basis functions, which can be calculated exactly for the VHS model. To balance the accuracy and the computational cost, a new collision model is built with a combination of the quadratic collision term and a linearized collision operator. Finally, several benchmark problems in the granular flow are implemented to validate the numerical method. Even for two-dimensional cases, this method can capture the behavior of inelastic gas flow well with high efficiency.

## Acknowledgements

We thank Prof. Jingwei Hu from UW for her valuable suggestions. We thank Prof. Lei Wu from SUSTC for his help with the DSMC code. The work of Yanli Wang is partially supported by the National Natural Science Foundation of China (Grant No. 12171026, U2230402 and 12031013).

## A Proof of Theorem 1

In order to prove Thm. 1, we first introduce the lemma below:

**Lemma 3.** Define  $\mathbf{v} = \mathbf{h} + \frac{1}{2}\mathbf{g}$ ,  $\mathbf{w} = \mathbf{h} - \frac{1}{2}\mathbf{g}$ , then

$$H_\lambda(\mathbf{v})H_\kappa(\mathbf{w}) = \sum_{\kappa' + \lambda' = \kappa + \lambda} a_{l'_1 k'_1}^{l_1 k_1} a_{l'_2 k'_2}^{l_2 k_2} a_{l'_3 k'_3}^{l_3 k_3} H_{\lambda'}(\sqrt{2}\mathbf{h}) H_{\kappa'}\left(\frac{1}{\sqrt{2}}\mathbf{g}\right), \quad (\text{A.1})$$

where the coefficients  $a_{l'_d k'_d}^{l_d k_d}$  are defined in (3.6).

The proof of Lemma 3 can be referred to [25, Lemma 3]. Besides, we can derive the corollary

**Corollary 1.** Define  $\mathbf{v} = \mathbf{h} + \frac{1}{2}\mathbf{g}$ , then it holds that

$$H_\lambda(\mathbf{v}) = 2^{-\frac{|\lambda|}{2}} \sum_{\kappa' + \lambda' = \lambda} \frac{\lambda!}{\kappa'! \lambda'!} H_{\kappa'}(\sqrt{2}\mathbf{h}) H_{\lambda'}\left(\frac{1}{\sqrt{2}}\mathbf{g}\right). \quad (\text{A.2})$$

The proof is straightforward by letting  $\kappa = \mathbf{0}$  in (A.1). Then we can present the proof of Theorem 1.

*Proof of Theorem 1.* First, we rewrite (3.4) as

$$A_{\alpha, \lambda, \kappa} = \frac{1}{\alpha!} \int_{\mathbb{R}^3} \int_{\mathbb{R}^3} \int_{S^2} B(|\mathbf{g}|, \sigma) H_\lambda(\mathbf{v}) H_\kappa(\mathbf{v}_*) [H_\alpha(\mathbf{v}') - H_\alpha(\mathbf{v})] \omega(\mathbf{v}) \omega(\mathbf{v}_*) d\sigma d\mathbf{v} d\mathbf{v}_*. \quad (\text{A.3})$$

Define  $\mathbf{h} = \frac{\mathbf{v} + \mathbf{v}_*}{2} = \frac{\mathbf{v}' + \mathbf{v}'}{2}$  and notice  $\mathbf{g} = \mathbf{v} - \mathbf{v}_*$  is the relative velocity. Besides, with  $\mathbf{g}'$  defined in (3.8), we have

$$\begin{aligned} \mathbf{v} &= \mathbf{g} + \frac{1}{2}\mathbf{h}, & \mathbf{v}_* &= \mathbf{g} - \frac{1}{2}\mathbf{h}, & \mathbf{v}' &= \mathbf{g}' + \frac{1}{2}\mathbf{h}, \\ d\mathbf{g} d\mathbf{h} &= d\mathbf{v} d\mathbf{v}_*, & \omega(\mathbf{v}) \omega(\mathbf{v}_*) &= \omega\left(\frac{1}{\sqrt{2}}\mathbf{g}\right) \omega(\sqrt{2}\mathbf{h}). \end{aligned} \quad (\text{A.4})$$

Combining Lemma 3, Corollary 1 and (A.4), we can transform (A.3) into an integral with respect to  $\mathbf{g}$  and  $\mathbf{h}$ :

$$A_{\alpha, \lambda, \kappa} = 2^{\frac{|\alpha|}{2}} \sum_{\lambda' + \kappa' = \lambda + \kappa} \sum_{\mathbf{i} + \mathbf{j} = \alpha} \frac{1}{\mathbf{i}! \mathbf{j}!} a_{l'_1 k'_1}^{l_1 k_1} a_{l'_2 k'_2}^{l_2 k_2} a_{l'_3 k'_3}^{l_3 k_3} \gamma_{\kappa'}^{\mathbf{j}} \eta_{\lambda'}^{\mathbf{i}}, \quad (\text{A.5})$$

where  $\gamma_{\kappa'}^j$  is the integral of  $\mathbf{g}$  defined in (3.7), and  $\eta_{\lambda'}^i$  is the integral of  $\mathbf{h}$  defined by

$$\eta_{\lambda'}^i = \int_{\mathbb{R}^3} H_{\lambda'}(\sqrt{2}\mathbf{h}) H_i(\sqrt{2}\mathbf{h}) \omega(\sqrt{2}\mathbf{h}) d\mathbf{h} = \frac{\lambda'!}{2^{\frac{3}{2}}} \delta_{\lambda', i}, \quad (\text{A.6})$$

which can be calculated with the orthogonality (F.1). The proof is completed by substituting (A.6) into (A.5).  $\square$

## B The proof for VHS kernel

In this section, the proof to Lemma 2, Proposition 3 and 4 is proposed.

*Proof of Lemma 2.* From the recurrence relationship (F.3) of Hermite polynomials, the one-dimensional standard Hermite polynomial can be expanded as

$$\begin{aligned} H_{2n}(x) &= \sum_{k=0}^n \frac{(2n-1)!!}{(2n-2k-1)!!} (-1)^k C_n^k x^{2n-2k}, \\ H_{2n-1}(x) &= \sum_{k=0}^{n-1} \frac{(2n-1)!!}{(2n-2k-1)!!} (-1)^k C_{n-1}^k x^{2n-2k-1}. \end{aligned} \quad (\text{B.1})$$

Substituting (B.1) into (3.10), and let  $\mathcal{C}(\alpha_i, j_i), i = 1, 2, 3$  be the coefficient of  $x^{j_i}$  in  $H_{\alpha_i}(x)$ , it holds that

$$\mathcal{V}(\kappa, \alpha, \mu) = \sum_{\substack{\mathbf{j} \preceq \alpha \\ 2|(\alpha-\mathbf{j})}} \mathcal{C}(\alpha_1, j_1) \mathcal{C}(\alpha_2, j_2) \mathcal{C}(\alpha_3, j_3) \int_{\mathbb{R}^3} \mathbf{v}^\kappa \mathbf{v}^{\mathbf{j}} |\mathbf{v}|^\mu \omega(\mathbf{v}) d\mathbf{v}. \quad (\text{B.2})$$

With the spherical coordinate transform  $\mathbf{v} = (r\chi_1, r\chi_2, r\chi_3)$ , where  $r \in \mathbb{R}^+$  and  $\chi = (\chi_1, \chi_2, \chi_3) \in S^2$ , it holds that

$$\mathcal{V}(\kappa, \alpha, \mu) = (2\pi)^{-\frac{3}{2}} \sum_{\substack{\mathbf{j} \preceq \alpha \\ 2|(\alpha-\mathbf{j})}} \mathcal{C}(\alpha, \mathbf{j}) \int_0^\infty r^{2+\mu+|\mathbf{j}|+|\kappa|} \exp\left(-\frac{r^2}{2}\right) dr \int_{S^2} \chi_1^{j_1+\kappa_1} \chi_2^{j_2+\kappa_2} \chi_3^{j_3+\kappa_3} d\chi. \quad (\text{B.3})$$

With Lemma 1 and the property of the Gamma function, (B.3) is simplified as

$$\mathcal{V}(\kappa, \alpha, \mu) = (2\pi)^{-\frac{3}{2}} \sum_{\substack{\mathbf{j} \preceq \alpha \\ 2|(\alpha-\mathbf{j})}} \mathcal{C}(\alpha, \mathbf{j}) 2^{\frac{1+\mu+|\mathbf{j}|+|\kappa|}{2}} \Gamma\left(\frac{3+\mu+|\mathbf{j}|+|\kappa|}{2}\right) \mathcal{S}(\mathbf{j} + \kappa), \quad (\text{B.4})$$

Which finishes the proof.  $\square$

*Proof of Proposition 3.* To prove (3.15), we first expand  $H_\alpha(\mathbf{g}')$  using (B.1) as

$$H_\alpha(\mathbf{g}') = \sum_{\substack{\lambda \preceq \alpha \\ 2|(\alpha-\lambda)}} \mathcal{C}(\alpha_1, \lambda_1) \mathcal{C}(\alpha_2, \lambda_2) \mathcal{C}(\alpha_3, \lambda_3) (\mathbf{g}')^\lambda. \quad (\text{B.5})$$

The binomial expansion of  $(\mathbf{g}')^\lambda$  holds that

$$(\mathbf{g}')^\lambda = \sum_{\kappa \preceq \lambda} C_\lambda^\kappa \left(\frac{1-e}{2}\right)^{|\kappa|} \left(\frac{1+e}{2}\right)^{|\lambda|-|\kappa|} \mathbf{g}^\kappa |\mathbf{g}|^{|\lambda|-|\kappa|} \sigma^{\lambda-\kappa}. \quad (\text{B.6})$$



From Lemma 1, we can derive that

$$\int_{S^2} \sigma^{\lambda-\kappa} \neq 0, \quad \text{if and only if } 2|(\lambda - \kappa). \quad (\text{B.7})$$

Combining (3.12), (B.6) and (B.7), we can directly derive (3.15). For (3.17), the proof is straightforward with the expansion of  $H_\alpha(\mathbf{g})$  and  $\int_{S^2} 1d\sigma = 4\pi$ .  $\square$

*Proof of Proposition 4.* To prove this proposition, we begin from (3.12) and (3.13). From (B.6) and (B.7), we can deduce that  $\mathbf{g}^\kappa |\mathbf{g}|^{|\lambda|-|\kappa|}$  is a polynomial of  $\mathbf{g}$  with degree  $|\lambda|$ . With the orthogonality of Hermite polynomials, it holds that

$$D(\mathbf{j}, \kappa, 0) = 0, \quad \text{if } |\mathbf{j}| < |\kappa|.$$

When  $\mu = 0$ , it is obvious that  $\psi(\mathbf{j}, \kappa, 0)$  can be nonzero only when  $\mathbf{j} = \kappa$ . Thus, one can see from (3.14) that

$$\gamma_\kappa^{\mathbf{j}} = 0, \quad \text{if } \varpi = 1 \text{ and } |\mathbf{j}| < |\kappa|.$$

Finally, when  $|\alpha| < |\lambda| + |\kappa|$  in  $A_{\alpha, \lambda, \kappa}$ , it can be observed that  $|\kappa'| - |\mathbf{j}| = |\kappa| + |\lambda| - |\alpha| > 0$  in the summation (3.5). We complete the proof.  $\square$

## C Projection operator

In this section, we present the theorem of the projection operator between different expansion centers. We refer the readers to [16, Theorem 3.1] for the related proof and details of this projection algorithm.

**Theorem 6.** Suppose  $f(\mathbf{v}) \in \mathbb{F}$  is expanded with two different expansion centers  $[\bar{\mathbf{u}}^{(1)}, \bar{\theta}^{(1)}]$  and  $[\bar{\mathbf{u}}^{(2)}, \bar{\theta}^{(2)}]$ . From (2.18), we can compute these two sets of expansion coefficients as

$$\begin{aligned} f_\alpha^{[\bar{\mathbf{u}}^{(1)}, \bar{\theta}^{(1)}]} &= \frac{1}{\alpha!} \int H_\alpha^{\bar{\mathbf{u}}^{(1)}, \bar{\theta}^{(1)}}(\mathbf{v}) f(\mathbf{v}) d\mathbf{v} \\ f_\alpha^{[\bar{\mathbf{u}}^{(2)}, \bar{\theta}^{(2)}]} &= \frac{1}{\alpha!} \int H_\alpha^{\bar{\mathbf{u}}^{(2)}, \bar{\theta}^{(2)}}(\mathbf{v}) f(\mathbf{v}) d\mathbf{v} \end{aligned} \quad (\text{C.1})$$

Then we have

$$f_\alpha^{[\bar{\mathbf{u}}^{(2)}, \bar{\theta}^{(2)}]} = \left( \bar{\theta}^{(2)} \right)^{-\frac{|\alpha|}{2}} \sum_{l=0}^{|\alpha|} \phi_\alpha^{(l)}, \quad (\text{C.2})$$

where  $\phi_\alpha^{(l)}$  is defined recursively by

$$\phi_\alpha^{(l)} = \begin{cases} \left( \bar{\theta}^{(1)} \right)^{\frac{|\alpha|}{2}} f_\alpha^{[\bar{\mathbf{u}}^{(1)}, \bar{\theta}^{(1)}]}, & l = 0, \\ \frac{1}{l} \sum_{d=1}^3 \left[ \left( \bar{\mathbf{u}}^{(2)} - \bar{\mathbf{u}}^{(1)} \right) \phi_{\alpha - e_d}^{(l-1)} + \frac{1}{2} \left( \bar{\theta}^{(2)} - \bar{\theta}^{(1)} \right) \phi_{\alpha - 2e_d}^{(l-1)} \right], & 1 \leq l \leq |\alpha|. \end{cases} \quad (\text{C.3})$$

In (C.3), terms with any negative index are regarded as 0.

## D WENO reconstruction

In this section, the WENO reconstruction for  $\mathbf{f}$  is listed, and the specific reconstruction coefficients are as below

$$\begin{aligned}
\mathbf{f}^{L,1} &= \frac{3}{2}\mathbf{f}_j^n - \frac{1}{2}\mathbf{f}_{j-1}^n, & \mathbf{f}^{L,2} &= \frac{1}{2}\mathbf{f}_j^n + \frac{1}{2}\mathbf{f}_{j+1}^n, \\
\mathbf{f}^{R,1} &= \frac{3}{2}\mathbf{f}_j^n - \frac{1}{2}\mathbf{f}_{j+1}^n, & \mathbf{f}^{R,2} &= \frac{1}{2}\mathbf{f}_j^n + \frac{1}{2}\mathbf{f}_{j-1}^n, \\
\omega_{L,1} &= \frac{\gamma_1}{\left[\varepsilon + (\mathbf{f}_j^n - \mathbf{f}_{j-1}^n)^2\right]^2}, & \omega_{L,2} &= \frac{\gamma_2}{\left[\varepsilon + (\mathbf{f}_{j+1}^n - \mathbf{f}_j^n)^2\right]^2}, \\
\omega_{R,1} &= \frac{\gamma_1}{\left[\varepsilon + (\mathbf{f}_{j+1}^n - \mathbf{f}_j^n)^2\right]^2}, & \omega_{R,2} &= \frac{\gamma_2}{\left[\varepsilon + (\mathbf{f}_j^n - \mathbf{f}_{j-1}^n)^2\right]^2}, \\
\mathbf{f}_{j+1/2}^{n,L} &= \frac{\omega_{L,1}\mathbf{f}^{L,1} + \omega_{L,2}\mathbf{f}^{L,2}}{\omega_{L,1} + \omega_{L,2}}, & \mathbf{f}_{j-1/2}^{n,R} &= \frac{\omega_{R,1}\mathbf{f}^{R,1} + \omega_{R,2}\mathbf{f}^{R,2}}{\omega_{R,1} + \omega_{R,2}}, \\
\varepsilon &= 10^{-6}, & \gamma_1 &= \frac{1}{3}, & \gamma_2 &= \frac{2}{3},
\end{aligned} \tag{D.1}$$

where the square of  $\mathbf{f}$  in (D.1) indicates squaring by each element and the superscript  $[\bar{\mathbf{u}}, \bar{\theta}]$  on  $\mathbf{f}$  is omitted.

## E Nondimensionalization

In this section, we provide the nondimensionalization to scale the variables as

$$\hat{\mathbf{x}} = \frac{\mathbf{x}}{x_0}, \quad \hat{\mathbf{v}} = \frac{\mathbf{v}}{u_0}, \quad \hat{t} = \frac{t}{x_0/u_0}, \quad \hat{m} = \frac{m}{m_0}, \quad \hat{f} = \frac{f}{\rho_0/(m_0 u_0^3)}, \quad \hat{B} = \frac{B}{B_0}, \tag{E.1}$$

where  $x_0$ ,  $\rho_0$ , and  $m_0$  are the characteristic length, density and mass. Besides,  $u_0$  is the characteristic velocity defined as  $u_0 = \sqrt{k_B \theta_0 / m_0}$  with  $\theta_0$  the characteristic temperature. Besides,  $B_0 = \sqrt{2} u_0 \pi d_{\text{ref}}^2$  is adopted to rescale the HS collision kernel, where  $d_{\text{ref}}$  is the reference diameter.

The characteristic parameters utilized for Argon and the HS model are listed in Tab. 3, where  $d_{\text{ref}}$  is derived with [4, Eq. (4.62)].

## F Properties of Hermite polynomials

For the Hermite polynomials (2.16), several important properties are listed below

**Property 1.** (*Orthogonality*)

$$\int_{\mathbb{R}^3} H_{\alpha}^{\bar{\mathbf{u}}, \bar{\theta}}(\mathbf{v}) H_{\beta}^{\bar{\mathbf{u}}, \bar{\theta}}(\mathbf{v}) \omega_{\bar{\mathbf{u}}, \bar{\theta}}(\mathbf{v}) d\mathbf{v} = \alpha_1! \alpha_2! \alpha_3! \delta_{\alpha, \beta}. \tag{F.1}$$

**Property 2.** (*Transitivity*)

$$H_{\alpha}^{\bar{\mathbf{u}}, \bar{\theta}}(\mathbf{v}) = H_{\alpha}^{0, \zeta} \left( \sqrt{\frac{\zeta}{\bar{\theta}}} (\mathbf{v} - \bar{\mathbf{u}}) \right). \tag{F.2}$$

Characteristic parameters for Argon:	
Characteristic mass $m_0$ ( $\times 10^{-26}$ kg)	6.63
Characteristic length $x_0$ (m)	$10^{-3}$
Characteristic velocity $u_0$ (m/s)	238.377
Characteristic temperature $\theta_0$ (K)	273
Parameters for HS model:	
Molecular mass: $m$ ( $\times 10^{-26}$ kg)	6.63
Ref. viscosity: $\mu_{\text{ref}}$ ( $\times 10^{-5}$ Pa s)	2.117
Viscosity index: $\varpi$	0.5
Scattering parameter: $\alpha$	1
Ref. diameter: $d_{\text{ref}}$ ( $\times 10^{-10}$ m)	3.63
Ref. temperature: $T_{\text{ref}}$ (K)	273

Table 3: (Nondimensionalization in App. E) Characteristic parameters in inhomogeneous tests.

**Property 3.** (*Recurrence*)

$$\begin{aligned}
H_{\alpha+e_d}^{\bar{\mathbf{u}},\bar{\theta}}(\mathbf{v}) &= \frac{v_d - u_d}{\sqrt{\bar{\theta}}} H_{\alpha}^{\bar{\mathbf{u}},\bar{\theta}}(\mathbf{v}) - \alpha_d H_{\alpha-e_d}^{\bar{\mathbf{u}},\bar{\theta}}(\mathbf{v}), \\
v_d H_{\alpha}^{\bar{\mathbf{u}},\bar{\theta}} &= \sqrt{\bar{\theta}} H_{\alpha+e_d}^{\bar{\mathbf{u}},\bar{\theta}} + u_d H_{\alpha}^{\bar{\mathbf{u}},\bar{\theta}} + \alpha_d \sqrt{\bar{\theta}} H_{\alpha-e_d}^{\bar{\mathbf{u}},\bar{\theta}}.
\end{aligned} \tag{F.3}$$

**Property 4.** (*Differential of Hermite polynomial*)

$$\frac{\partial}{\partial v_d} H_{\alpha}^{\bar{\mathbf{u}},\bar{\theta}}(\mathbf{v}) = \frac{\alpha_d}{\sqrt{\bar{\theta}}} H_{\alpha-e_d}^{\bar{\mathbf{u}},\bar{\theta}}(\mathbf{v}). \tag{F.4}$$

The property of transitivity can be directly derived from the definition (2.16), and the proof of the other properties can be found in [1].

## References

- [1] M. Abramowitz and I. Stegun. Handbook of mathematical functions with formulas, graphs, and mathematical tables. *New York: Dover*, 1964.
- [2] A. Astillero and A. Santos. Uniform shear flow in dissipative gases: Computer simulations of inelastic hard spheres and frictional elastic hard spheres. *Phys. Rev. E*, 72(3):1–23, 2005.
- [3] P. Bhatnagar, E. Gross, and M. Krook. A model for collision processes in gases. i. small amplitude processes in charged and neutral one-component systems. *Phys. Rev.*, 94(3):511–525, 1954.
- [4] G. Bird. *Molecular Gas Dynamics and the Direct Simulation of Gas Flows*. Oxford: Clarendon Press, 1994.
- [5] N. Brilliantov and T. Poschel. *Kinetic Theory of Granular Gases*. Oxford University Press, 2004.

- [6] Z. Cai. *Investigations and Applications of the Numerical Moment Method in the Kinetic Theory of Gases (in Chinese)*. PhD thesis, Peking University, June 2013.
- [7] F. Filbet and T. Rey. A rescaling velocity method for dissipative kinetic equations. Applications to granular media. *J. Comput. Phys.*, 248:177–199, 2013.
- [8] I. Gamba, J. Haack, C. Hauck, and J. Hu. A fast spectral method for the Boltzmann collision operator with general collision kernels. *SIAM J. Sci. Comput.*, 39(14):B658–B674, 2017.
- [9] I. Gamba, S. Rjasanow, and W. wagner. Direct simulation of the uniformly heated granular boltzmann equation. *Math. Comput. Model.*, 42:683–700, 2005.
- [10] H. Grad. On the kinetic theory of rarefied gases. *Comm. Pure Appl. Math.*, 2(4):331–407, 1949.
- [11] P. Haff. Grain flow as a fluid-mechanical phenomenon. *J. Fluid Mech.*, 134:401–430, 1983.
- [12] A. Harten, P. Lax, and B. Leer. On upstream differencing and Godunov-type schemes for hyperbolic conservation laws. *SIAM Review*, 25(1):35–61, 1983.
- [13] L. Holway. New statistical models for kinetic theory: Methods of construction. *Phys. Fluids*, 9(1):1658–1673, 1966.
- [14] J. Hu and Z. Ma. A fast spectral method for the inelastic boltzmann collision operator and application to heated granular gases. *J. Comput. Phys.*, 385:119–134, 2019.
- [15] J. Hu, J. Shen, and Y. Wang. A Petrov–Galerkin spectral method for the inelastic Boltzmann equation equation using mapped Chebyshev functions. *Kinet. Relat. Models*, 13(4):677–702, 2020.
- [16] Z. Hu, Z. Cai, and Y. Wang. Numerical simulation of microflows using Hermite spectral methods. *SIAM J. Sci. Comput.*, 42(1):B105–B134, 2020.
- [17] R. Li, Y. Lu, Y. Wang, and H. Xu. Hermite spectral method for multi-species Boltzmann equation. *J. Comput. Phys.*, 471:111650, 2022.
- [18] R. Li, Y. Ren, and Y. Wang. Hermite spectral method for Fokker-Planck-Landau equation modeling collisional plasma. *J. Comput. Phys.*, 434:110235, 2021.
- [19] C. Liu, Z. Wang, and K. Xu. A unified gas-kinetic scheme for continuum and rarefied flows VI: dilute disperse gas-particle multiphase system. *J. Comput. Phys.*, 386:264–295, 2019.
- [20] X. Liu, S. Osher, and T. Chan. Weighted essentially non-oscillatory schemes. *J. Comput. Phys.*, 115:200–212, 1994.
- [21] C. Mouhot and L. Pareschi. Fast algorithms for computing the Boltzmann collision operator. *Math. Comp.*, 75(256):1833–1852, 2006.
- [22] L. Pareschi and G. Toscani. *Interacting Multiagent Systems*. Oxford University Press, UK, 2014.
- [23] T. van Noije and M. Ernst. Velocity distributions in homogeneous granular fluids: the free and the heated case. *Granul. Matter*, 1:57–64, 1998.

- [24] C. Villani. Mathematics of granular materials. *J. Stat. Phys.*, 124:781–822, 2006.
- [25] Y. Wang and Z. Cai. Approximation of the Boltzmann collision operator based on hermite spectral method. *J. Comput. Phys.*, 397:108815, 2019.
- [26] L. Wu, Y. Zhang, and J. Reese. Fast spectral solution of the generalized enskog equation for dense gases. *J. Comput. Phys.*, 303:66–79, 2015.